aerospace

MDPI

Article

Numerical Investigation of Nanofluid Flow over a Backward Facing Step

Wen-Chung Wu * and Ankit Kumar

Department of Aeronautical Engineering, National Formosa University, Huwei, Yunlin 632, Taiwan
* Correspondence: wuwenj@nfu.edu.tw

Abstract: Nanofluid flow over a backward facing step was investigated numerically at low Reynolds number and the heat transfer was analyzed and reported. Al_2O_3–H_2O nanofluids of different volume fractions (φ = 1–5%) were used as the material with uniform heat flux (UHF) of 5000 W/m^2 at bottom wall for Reynolds number 200–600. The backward facing step of two geometries was investigated for two expansion ratios, 1.9432 and 3.5. The SIMPLE algorithm was used in the finite volume solver to solve the Naiver–Stokes equation. Temperature difference at inlet and boundaries, heat transfer coefficient, Nusselt number, coefficient of skin friction, and temperature contours were reported. The results show that when nanofluids are used, the coefficient of heat transfer and Nusselt number increased at all volume fractions and Reynolds number for both the expansion ratios. The coefficient of heat transfer at φ = 5% was higher by 9.14% and 9.68% than the pure water for ER = 1.9432 and ER = 3.5 at Re. 500. At φ = 5%, the outlet temperature for the duct decreased by 10 K and 5 K when compared to the pure water for ER = 1.9432 and ER = 3.5 at Re. 500. Coefficient of skin friction and outlet temperature decreased for both the volume fractions in both the expansion ratios.

Keywords: nanofluid; heat transfer; Nusselt number

check for updates

Citation: Wu, W.-C.; Kumar, A. Numerical Investigation of Nanofluid Flow over a Backward Facing Step. *Aerospace* **2022**, *9*, 499. https://doi.org/10.3390/aerospace9090499

Academic Editor: Pietro Catalano

Received: 25 July 2022
Accepted: 29 August 2022
Published: 7 September 2022

1. Introduction

In chemical, mechanical, biomedical, and power generation industries, heat transfer is one of the most important parameters for investigation as it decides the thermal performance and efficiency of the system. One of the latest and recent innovations to improve the thermophysical properties of the conventional fluids such as water, ethyl alcohol, and oil has been to use nanofluids. A nanofluid is a solution with a higher heat transfer rate, which is used in many industries. Nanofluids are colloidal suspensions of nanoparticles and a base fluid which gives the mixture enhanced thermal properties. It is used in radiators, electronic cooling systems, and in heat exchangers as coolants. Nanofluids have a great potential in transportation for improving automotive and heavy-duty engine cooling rate by increasing the efficiency, decreasing the weight and also reducing complexity of the thermal management system. The greater the specific area, the more heat transfer surface between the base fluid and the nanoparticle. The thermal properties of the nanofluid can be adjusted according to the requirements by varying the particle concentrations. Studies by Choi [1] have shown that a small quantity of nanoparticles could increase the thermal conductivity to a larger extent. Nano-sized particles generally of metals, carbides, oxides, or carbon nanotubes are mixed with the base fluids. The nanofluids exhibit a higher thermal property than the conventional coolants and increase the stability of the suspension. Nanoparticles are produced by different processes such as chemical precipitation, mechanical attrition, gas condensation, laser ablation, and spark ablation. Nanofluids can be produced by direct evaporation, chemical precipitation, gas condensation/dispersion, etc. Hybrid nanofluids have also been studied in order to understand the heat transfer and analyze if they have a higher heat transfer capability.

The backward facing step (BFS) is a representative of flow separation models which has both academic and industrial significance. Separation flows can be seen in aerodynamics when the fluid flows past airfoil, spoilers and behind the vehicle. Flow separation studies are of extreme importance because of their application in cooling the turbine blades, air condition networks, combustor, fluid transmission lines, condenser, flow passing through the engine, and many other devices. Flow separation, vortex evolution, and flow reattachment occur when the flow passes over a backward facing step. When flow passes near the boundaries having corners, vortices are generated near the corners. This phenomenon was predicted by Moffatt [2]. Studies have been done to understand the length of the region where the vortices are generated for various geometries having corners. The flow for backward facing step has also been studied where the research has been focused mainly on the dependence on Reynolds number. The early studies by Roache [3], Durst and Pereira [4], and Taylor and Ndefo [5] predicted that the separation is not observed at the upper corner of the step at low Reynolds number flow. The research was done for low Reynolds numbers and the behavior of the vortex's generation was analyzed. Experiments and numerical simulations of laminar, transitional, and turbulent flows with a separation region behind a 2D backward-facing step were performed by Armaly et al. [6]. Flow behavior over backward facing step for varying expansion ratios were investigated numerically to understand the flow separation and reattachment by Biswas et al. [7]. Both 2D and 3D simulations were performed to analyze the length of reattachment in case of higher Reynolds number to study the justification given by Armaly et al. [6] regarding the deviation when comparing the experimental and numerical results. The results show that the Moffatt eddies are not just generated at $Re \rightarrow 0$ but is also generated at $Re = 1$. The primary recirculation length is found to increase non-linearly with increasing expansion ratio.

Abedalh et al. [8] experimentally investigated a nanofluid by using Al_2O_3 and TiO_2 nanoparticles with pure water as base fluid. The nanofluid was investigated for 1%, 2%, and 3% mass fraction. Pressure drop and enhancement in the heat transfer were analyzed for flow over backward facing step inside a heated rectangular duct. The results showed that the Nusselt number increases and the friction factor decreases with increase in Reynolds number. Al_2O_3 and TiO_2 were used as nanoparticles for a water based nanofluid by Klazy and Bognar [9] to study the effect of change in temperature in a micro-sized backward facing step. The results show that the rate of heat transfer increased with increasing volume fraction. The velocity was also reported to increase with the increase in temperature difference. The size of the recirculation zone also increased with higher temperature difference. Water–Al_2O_3 nanofluid flow in a micro backward facing step was simulated numerically by Klazly et al. [10] by considering the fluid behavior as Newtonian and non-Newtonian at volume fractions ranging between 1 and 4%. A higher heat transfer has been predicted when the nanoparticles are added and the Newtonian fluid shows a higher coefficient of heat transfer than non-Newtonian fluid.

A finite volume approach and k-epsilon standard turbulence model was used for investigating the effect of Reynolds number, step, and liquid type in enhancing the heat transfer by Abdulrazzaq et al. [11]. The backward facing expanding channel was used and three liquids, i.e., ethylene glycol, liquid ammonia, and water, were considered for the flow. The result shows an increase in local Nusselt number with the increasing Reynolds number. Coefficient of skin friction was also reported for various steps of the downstream section. Cu-water nanofluids were investigated numerically by Safaei et al. [12] by changing the expansion angles in a microtube and heat transfer characteristics were reported. Increasing Reynolds number has shown an increase in coefficient of heat transfer and pressure drop. A maximum increase of 28.1% in coefficient of heat transfer was reported for $\varphi = 4\%$ nanofluid. This research, after further detailed investigation, could be manufactured for new types of solar receivers. Symmetry simulation of the hybrid nanofluid flow was also investigated by Goldanlou et al. [13] and heat transfer was analyzed for an annulus with cold and hot rods. The symmetry simulation for hybrid nanofluid flow has not been attempted before. The hybrid nanofluid is an ethylene–glycol, water, or water/ethylene–glycol-based mixture of Cu-Al_2O_3. Higher average Nusselt number has been reported with increase in Reynolds number. The high emissivity values should have led to a high radiation heat transfer but a portion of the radiative heart transfer is very low in the annulus leading to an almost negligible observed increase in the fluid flow and heat transfer.

Heat transfer and friction factor have been investigated for nanofluid flow over the backward facing step by Hilo et al. [14]. A nanofluid was prepared by CuO and MgO-EG at a dimeter of 40 nm nanoparticles and EG as the base fluid at varying volume concentration from 0% to 5% for Reynolds number between 5000 and 20,000. The nanofluid enters the test channel and passes over backward facing step. Heat flux is applied at the bottom wall of the channel which increase the temperature of the working fluid. As the volume fraction increases, the local Nusselt number increases. At the lowest volume concentration of nanoparticles (0.01), a slight decrease in local Nusselt number was observed since the increase in thermal conductivity of the nanofluid at volume concentration 0.01 is less than the increase in viscosity. For all the examined cases, the friction factor tends to increase as the volume fraction of increases. The friction factor decreases as the Reynolds number increases regardless of the volume concentration of nanoparticles. Unsteady flow and natural convection heat transfer of the fractional Maxwell viscoelastic fluid over the sudden expansion geometry such as a backward facing step was investigated by Moosavi et al. [15]. Nonlinear boundary layer governing equations with the fractional derivative Maxwell model was used for the current investigation. The time–space fractional derivatives were calculated based on the Caputo and nonlinear governing equations solved through finite difference method mixed with L-1 algorithm. Maxwell model describes the rheological effects of the viscoelastic fluid as reported by Careglio et al. [16–18]. The results showed that the temperature and velocity boundary layers increased with increasing fractional derivative parameters. With increasing dimensionless temperature, heat transfer and the coefficient of friction increases. As the length of the backward facing step is increased, the average Nusselt number, coefficient of friction, velocity, and temperature boundary layer thickness increase. Nusselt number for Maxwell fluid flow is higher than the Newtonian fluid flow. Thermal conductivity of the Maxwell flow is lowest while the thermal boundary layer thickness is lowest for the Newtonian fluid.

Magnetized hybrid nanofluid was investigated by Lund et al. [19] where temporal stability analysis was performed. Kolsi [20] used magnetic field for the investigation of the nanofluid flow in a backward facing step by finite element method. Two rotating cylinders were placed in the backward facing step and the simulations were performed for various volume fractions. The rotating cylinders made the flow field much more complex and the vortices on the upper and lower channel walls were suppressed due to the magnetic field. The Nusselt number increased with the increase in Reynolds number and the values became higher when the first cylinder was rotating clockwise. Nanofluid flow past cylinders were also investigated by multiple researchers to understand the heat transfer characteristic and the flow field as the vortex shedding happens. A hybrid nanofluid was used as the working fluid by [21–31], and conventional nanofluids by [32–40]. In conventional nanofluids, the majority of the nanoparticles used were aluminum, silver, copper, and iron in metallic nanoparticles and Al_2O_3, CuO, Fe_3O_4, SiO_2, and TiO_2 in nonmetallic nanoparticles. Although the most commonly investigated base fluid is water, many investigations have considered ethylene glycol and oil.

Cao et al. [41] studied the unsteady boundary layer flow and the heat transfer of fractional Maxwell viscoelastic nanofluid over a plate in motion. The fractional Maxwell model was extended to analyze the flow and heat transfer of viscoelastic nanofluid. L-1 algorithm was also used here combined with the governing equations for fractional derivatives dependent on time in convection terms and were solved by the finite difference method. The results showed that temperature and velocity relaxation time enhance the heat transfer and convection flow, while the temperature and velocity fractional derivative parameters have an opposite effect. As the temperature and velocity fractional derivative parameters increased, average Nusselt number increased, while average coefficient of skin friction was influenced only by velocity fractional derivative parameter. Nanofluid flow towards the stagnation region of the shrinking cylinder has been numerically investigated by Waini [42] to analyze the thermal behavior by employing the correlations by Ho et al. [43]. A unique solution was reported for the shrinking strength. The rate of heat transfer and the friction factor showed an increase with increasing volume fraction and curvature parameter. Hybrid nanofluids were also researched for further enhancement of heat transfer. Takabi and Salehi [44] reported the hybrid nanofluid thermophysical models, which were used for boundary layer problems by [19,45–48].

A 2D laminar and turbulence mixed convection nanofluid flow over a backward facing step inside a heated rectangular duct with a baffle on the wall were investigated by Mohammad et al. [49]. The effect on the flow due to the baffle and heat transfer characteristics were analyzed while heating the duct's bottom with a constant heat flux. Four nanofluids namely, Al_2O_3, CuO, SiO_2, and ZnO of different volume fractions and the nanoparticle diameters of 25 to 80 nm were investigated. The highest Nusselt number was achieved for SiO_2, which is followed by Al_2O_3, ZnO, CuO, and pure water. Nath and Krishnan [50] performed numerical simulation for mixed convective heat and mass transfer in the backward facing channel with Cu-H_2O nanofluid. The effect of nanoparticles was analyzed using the Maxwell–Garnett model assuming that nanoparticles have a spherical shape. With increase in volume fraction of the nanoparticles, length of reattachment increased which was pronounced with the increasing Prandtl number from 1.76 to 6.2. The average Sherwood number decreased by 21% with increase in volume fraction of nanoparticles at Prandtl number = 1.76, which is a reverse trend observed for the average Nusselt number and the percentage was increased up to 34% at Pr = 6.2. A numerical investigation of ethylene glycol–SiO_2 nanofluid flow and heat transfer of laminar mixed convection over 3D, horizontal microscale forward-facing step was performed by Kherbeet et al. [51]. The forward-facing step increased the heat transfer and the Nusselt number increased with increasing step height. The results also showed no effect on the heat transfer at inclination angles. Kherbeet et al. [52] also carried out an experimental study for microscale forward and backward facing steps with water–SiO_2 nanofluid and found that at 0.01 concentration, the nanofluid showed the highest Nusselt number for the forward-facing steps.

Pulsating flow has been studied by many researchers [53–58] as it is one of the most important methods to enhance the thermal characteristics. Pulsating CuO–water nanofluid flow over the backward facing step with a corrugated bottom wall has been investigated numerically at constant temperature by Selimefendigil and Oztop [59]. Effect of height and length of surface corrugation wave, the volume fraction of nanoparticle, Reynolds number, frequency and amplitude of pulsation on the fluid flow, and the heat transfer were examined. The results showed that existence of additional surface corrugation waves led to a less effective process of heat transfer. Average Nusselt number was enhanced with the flow pulsation amplitude. The resonance-type behavior was seen for spatial-temporal average Nusselt number vs. Strouhal number plot which was observed in a previous study of the pulsating flow in the channel. Average Nusselt number increased with inclusion of nanoparticles but the rate of increase depends on the nanoparticle solid volume fraction (VF) interval. A computational methodology based on a proper orthogonal decomposition and ANN modeling of the modal coefficients that could be used rather than the high fidelity parametric unsteady CFD simulations was developed and the results were compared. Pulsating nanofluid flow over the backward facing step was numerically investigated by Chamkha and Selimefendigil [60] using different particle shapes. Three different nanoparticle shapes were investigated, i.e., blade, spherical, and cylindrical. SiO_2 nanofluid was used with a pulsation amplitude of 0.6. The recirculation zone behind the backward facing step were affected for different nanoparticle shapes. For all the investigated cases, the Nusselt number is a decreasing function of the Strouhal number and an increasing function of nanoparticle volume fraction. The average Nusselt number increases by 27.95% and 30.24% for the flow when the nanoparticle is of spherical and cylindrical shape at volume fraction 4%. The spherical nanoparticles were found optimal for pulsating flow and the cylindrical particles were found optimal for the constant flow. Zahmatkesh and Torshizi [54] investigated unsteady pulsating flow and heat transfer of nanofluid with silver nanoparticles. The simulation was performed for flow over a backward facing step using two-phase Eulerian–Eulerian model. They found that the increased pulse amplitude and frequency resulted in higher penetration of nanoparticles leading to an augmented heat transfer. Selimefendigil and Oztop [55] studied forced heat transfer for a pulsating nanofluid flow on a backward facing step with a wavy bottom. They developed efficient numerical methods to predict the efficiency of the heat transfer by neural networks and orthogonal decomposition with the attained results. Not a lot of experiments have been done for pulsating flows as the suitable equipment is lacking but recently, velocity measurements have become easy for pulsating flows as new technologies are coming.

Wang et al. [61] used k-ε and LES models for specific geometry of backward facing step for analysis and results were validated with DNS and PIV measurements at Reynolds number 9000. The results showed that the LES model could not effectively simulate boundary layer near the wall areas without extremely fine mesh and it tends to overestimate separation at top wall. These resulted in the Reynolds stresses, static pressure, mean velocity, and turbulent kinematic energy to show a larger peak value when compared to other methods. LES model could effectively simulate instantaneous large-scale vortices in backward facing step flow. Direct numerical simulation of the vorticial structure along the bottom wall of a backward facing step was performed and the effect on the enhancement of heat transfer in transitional flow over the backward facing step was analyzed by Xie et al. [62]. Research on transitional flow was performed by [63,64], but very little research has been done to investigate the heat transfer characteristics. The results show an increase in heat transfer for Reynolds number 700 and the highest value of Nusselt number was achieved at Reynolds number 1200. A vortical structure was generated due to the flow instability which destroys the boundary layer and rotates the colder fluid to the bottom wall, thus enhancing the heat transfer in the transitional flow regime.

Apart from hybrid nanofluids, carbon nanotubes are also used as nanoparticles with base fluids to enhance the thermal properties of the resultant nanofluids. The nanoparticles, other than having a very good thermal properties, also have radiation absorbing properties. Single-walled carbon nanotubes and multiwall carbon nanotubes have been used as nanoparticles for investigating the heat transfer characteristics. Alrased et al. [65] studied the nanofluid flow and heat transfer of water/functional multiwalled carbon nanotubes (FMWCNT) numerically inside a backward contracting channel. The effect of heat flux on the wall and the Reynolds number were investigated. A decrease in velocity led to decrease in pressure drop, coefficient of heat transfer, and coefficient of friction. Addition of nanoparticles at higher Reynolds number seems significant as it affects the thermal properties. Vortex generation at higher Reynolds number has also been discussed. Safaei et al. [66] also investigated the FMWCNT at various Reynolds numbers and heat fluxes in a forward-facing contracting channel numerically.

The research on nanofluid flow over the backward facing step has been done by many researchers but most of the research was done for turbulent flow regime. The heat transfer at turbulent flow regime becomes higher as the turbulence plays a major role. Very little research has been found to be for flow in a laminar regime at very low Reynolds number. The analysis helps in understanding various separation flow physics to predict the resultant flow. The current research focusses on nanofluid flow in the laminar flow regime over backward facing step in a duct by applying a uniform heat flux on bottom wall.

2. Governing Equations and Nanofluid Properties

2.1. Governing Equations

The incompressible viscous fluid flow equations are governed by equation of conservation of mass and the two components of the momentum equation in two dimensions. An additional energy equation was used to compute heat transfer and temperature.

$$\frac{\partial u}{\partial x} + \frac{\partial v}{\partial y} = 0 \tag{1}$$

$$u\frac{\partial u}{\partial x}+v\frac{\partial v}{\partial y}=-\frac{1}{\rho}\frac{\partial p}{\partial x}+\frac{\mu}{\rho}\left(\frac{\partial^2 u}{\partial x^2}+\frac{\partial^2 u}{\partial y^2}\right)+F_b+F_s \tag{2}$$

$$u\frac{\partial u}{\partial x}+v\frac{\partial v}{\partial y}=-\frac{1}{\rho}\frac{\partial p}{\partial y}+\frac{\mu}{\rho}\left(\frac{\partial^2 v}{\partial x^2}+\frac{\partial^2 v}{\partial y^2}\right)+F_b+F_s \tag{3}$$

$$C_p\left(u\frac{\partial T}{\partial x}+v\frac{\partial T}{\partial y}\right)=\frac{K}{\rho}\left(\frac{\partial^2 T}{\partial x^2}+\frac{\partial^2 T}{\partial y^2}\right) \tag{4}$$

The Equation (1) is continuity equation, (2) and (3) are the two momentum equations for both the x and y direction, and Equation (4) is the energy equation where u, v, ρ, F_b, F_s, and μ are velocity in x and y directions, density, body force, and viscosity.

2.2. Nanofluid

The nanofluid used for the current research consists of aluminum oxide also known as alumina (Al_2O_3) nanoparticles and water (H_2O) as base fluid. Thermal properties of materials are given in Table 1. The properties of the nanofluid at different volume fractions were calculated from Equations (5)–(9). The viscosity [67], density [68], thermal conductivity [69], and specific heat were calculated and the simulations were done in a single phase.

$$\mu_{nf}=\frac{\mu_f}{(1-\varphi)^{2.5}} \tag{5}$$

$$\rho_{nf}=\varphi\rho_{np}+(1-\varphi)\rho_f \tag{6}$$

$$k_{nf}=k_f\left[\frac{\left(k_p-2k_f\right)-2\varphi\left(k_f-k_{np}\right)}{\left(k_p-k_f\right)+\varphi\left(k_f-k_{np}\right)}\right] \tag{7}$$

$$(c_p)_{nf}=\frac{(1-\varphi)(\rho C_p)_f+\varphi(\rho C_p)_{np}}{(\rho)_{nf}} \tag{8}$$

$$Re_{nf}=\frac{\rho_{nf}\times v_{nf}\times d}{\mu_{nf}} \tag{9}$$

$$Nu_{avg.}=\frac{h_{average}\times d}{k_{nf}} \tag{10}$$

Table 1. Material properties.

Materials	Density	Thermal Conductivity	Specific Heat	Viscosity
Al_2O_3 [70,71]	3600	36	765	-
H_2O [71]	997.1	0.613	4179.1	0.001

The nanofluid properties have been defined through Equations (5)–(8) in which density, thermal conductivity, specific heat, and viscosity are calculated. The properties are calculated for simulation for a single-phase model. Equations (5)–(8) are the equations for viscosity, density, thermal conductivity, and specific heat where ρ, μ, c_p, k, and φ are density, viscosity, specific heat, thermal conductivity, and volume fraction. The subscript nf, np, and f represent nanofluid, nanoparticles, and base fluid. The inlet flow velocity is represented in terms of Reynolds number in Equation (9). The ratio of convective heat transfer to conductive heat transfer is denoted through a dimensionless term Nusselt number given in Equation (10).

3. Computational Domain and Grid Independence Study

Flow phenomena over the backward facing step is a highly researched topic as the flow downstream the step results in a very complex and interesting flow phenomena forming a recirculation region. The geometry has one backward facing step which has the total pipe length of 35 m. The backward facing step is located at 5 m from the inlet boundary. Figure 1 shows the problem geometry and a zoomed-out mesh selected for the numerical investigation. The height of backward facing step with respect to the total height of the pipe was defined through expansion ratio as described in Armaly et al. [6]. The expansion ratio was expressed in Equation (11). Two expansion ratios, 1.9432 and 3.5, were used for the current research.

$$E.R. = \frac{D}{d} \quad (11)$$

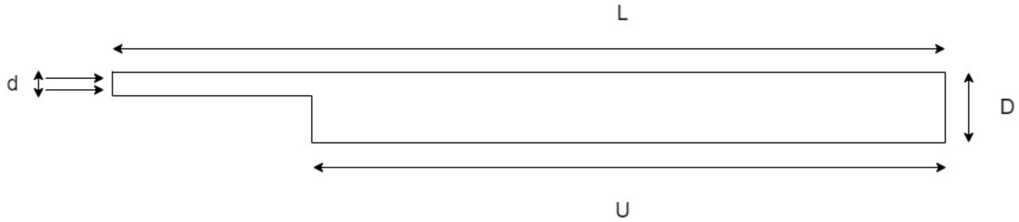

(**a**)

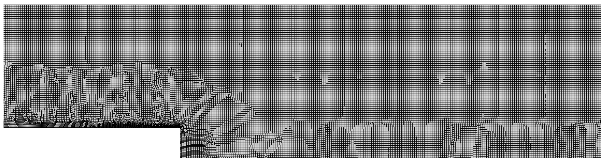

(**b**)

Figure 1. (**a**) Problem geometry; (**b**) computational mesh for ER—1.9432; (**b**) zoomed out computational mesh.

The computational grid was made with the quadrilateral dominant mesh having both the triangular and quadrilateral mesh as per the geometry. A very fine grid was generated at the lower wall to ensure that the resultant flow features near the wall boundary are in detail. A grid independence study was performed to select the most suitable grid so that the resultant value does not have high difference when the number of elements was varied. The results show that the difference in results for second and third grid were minimal when compared with the results of Biswas et al. [7] as shown in Table 2. A second grid was selected for the research as Table 2 shows that with increasing number of elements the difference in results was negligible. The details of the two meshes for expansion ratio are described in Table 3.

Table 2. Grid independence study at Reynolds number 100.

Mesh	No. of Elements	Length of Recirculation Zone	Biswas et al. [7]
1	101,656	2.735	
2	248,805	2.63	2.64
3	473,202	2.65	

Table 3. Selected mesh details.

Mesh	No. of Elements	Max. Skewness	Avg. Skewness
1	248,805	0.60092	0.024169
2	231,225	0.78036	0.027475

For the numerical simulation, a finite volume method solver was employed for computation. A SIMPLE scheme was selected for pressure velocity coupling to enforce the conservation of mass and obtaining pressure field. For spatial discretization, second order upwind was used for momentum and energy equations. The simulation was performed for laminar flow regime with a uniform heat flux (UHF) applied on bottom wall and the convergence criteria considered for simulations for all equations was 10^{-6}.

4. Code Validation

The first backward facing step of expansion ratio of 1.9432 was used for validating the model used. Pure water was used for the simulations at various Reynolds number. Water was used as the material for the numerical simulation. The length of recirculation region was calculated and results were validated with Armaly et al. [6], Biswas et al. [7], and Klazy and Bognar [70].

Figure 2 shows the length of recirculation region at varying Reynolds number for flow over backward facing step. The plot shows that current results very much agree with existing literature. Figure 3 shows streamlines for the simulation near the backward facing step. A vortex was generated after the flow passed the upper corner of step which then separated creating a recirculation region. When the Reynolds number was low as shown in Figure 3a–c, the flow separation did not occur at upper corner of the step. This flow regime mainly showed a creepy flow. When the Reynolds number reached 50 as in Figure 3d, the flow separation at the top corner occurred creating a significantly larger recirculation zone. Since the current results agree with the results from existing literature, the model was used for further research.

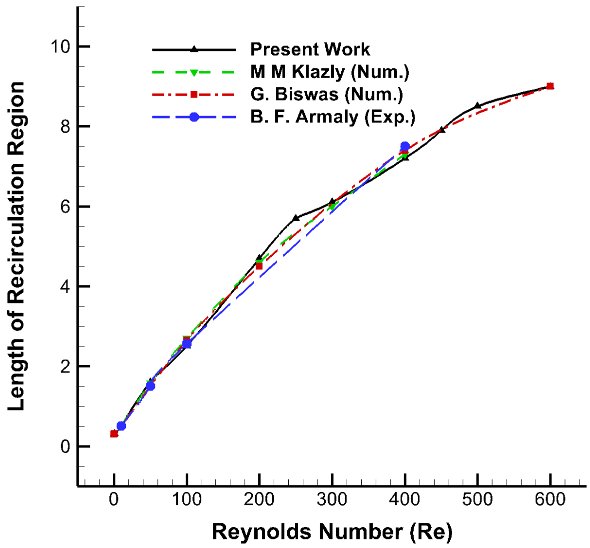

Figure 2. Length of the primary recirculation region behind backward facing step having an expansion ratio of 1.9423 for flow of water compared with Armaly [6], Biswas [7] and Klazly [71].

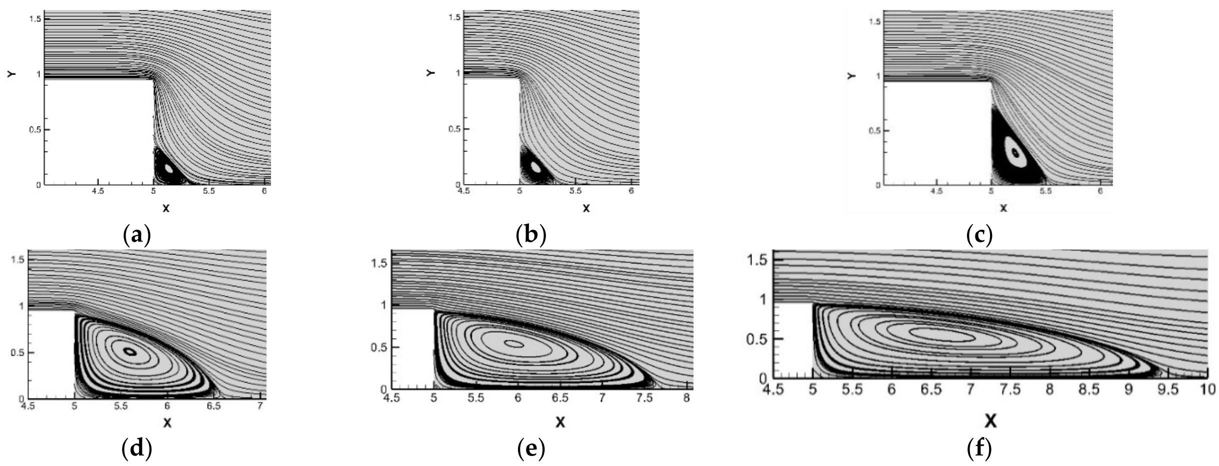

Figure 3. *Cont.*

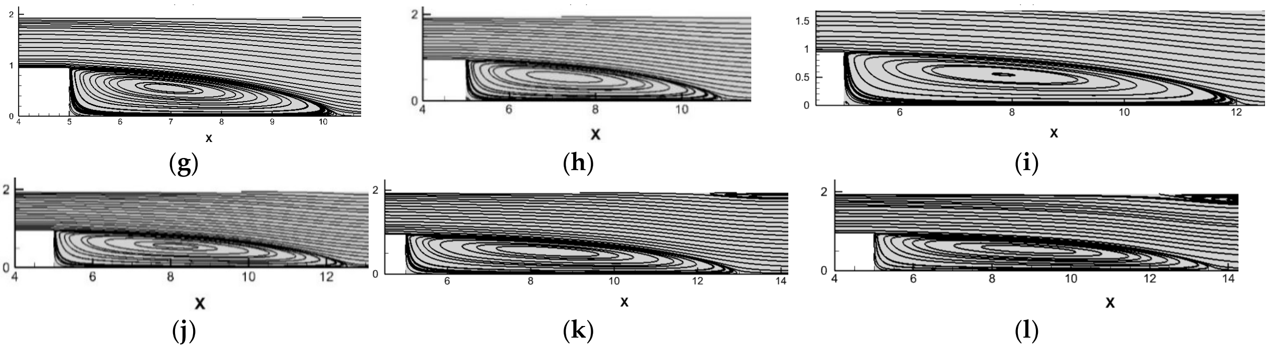

Figure 3. Streamlines near the backward facing step for flow of water at various Reynolds number: (**a**) 0.1, (**b**) 1, (**c**) 10, (**d**) 50, (**e**) 100, (**f**) 200, (**g**) 250, (**h**) 300, (**i**) 400, (**j**) 450, (**k**) 500, and (**l**) 600.

5. Results and Discussion

Flow over a backward facing step inside a duct at an expansion ratio of 1.9432 and a uniform heat flux (UHF) of 5000 W/m^2 at bottom wall with pure water as the material was performed. The simulations were performed for various Reynolds number and varying volume fraction from 1% to 5%. Two expansion ratios were considered for the current simulation. The properties of nanofluids, i.e., viscosity, density, thermal conductivity, and specific heat, were calculated. The nanofluids were used as materials and the inlet temperature was kept constant for all cases, i.e., 303 K. Heat transfer parameters were reported defining the change in heat transfer when comparing pure water and the nanofluid.

5.1. Pure Water Flow over Backward Facing Step at ER—1.9432

Flow past a backward facing step for pure water at varying Reynolds number was investigated and analyzed. Temperature contours were reported to analyze the visualize the change in temperature for the resultant flow, flow over the backward facing step and near the corners of the step. Heat transfer coefficient, Nusselt number, coefficient of skin friction, and the temperature along the bottom wall were reported for various Reynolds numbers.

Figure 4 shows the temperature contours at varying Reynolds number. The flow separated at the upper corner of the step and the temperature was higher at the vertical wall of step. The highest temperature was however at the lower corner of the step. The uniform heat flux was applied throughout the lower bottom wall of duct. The temperature in lateral direction increased along the bottom wall with increasing Reynolds number. The area of higher temperature increased and it became highest at Reynolds number 600 in Figure 4e. With increase in flow velocity, the highest temperature which was along the lateral side of the step started decreasing as shown in the contour with increasing Reynolds number. The longitudinal length up to which the temperature was higher decreased with the increase in the Reynolds number. The lateral height of the resultant flow also decreased with increase in Reynolds number.

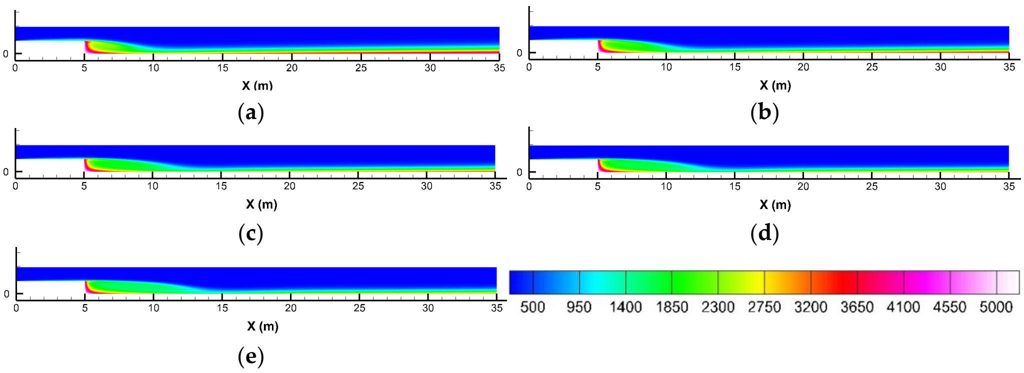

Figure 4. Temperature contours at various Reynolds numbers; (**a**) 200, (**b**) 300, (**c**) 400, (**d**) 500, and (**e**) 600.

Figure 5 shows the resultant heat transfer parameters for the simulations along the bottom wall length of the duct. The coefficient of heat transfer was found to increase with increasing Reynolds number. At the bottom wall, at the step, the heat transfer coefficient was about 6 w/m^2 K at the upper corner and about 1 w/m^2 K at the lower corner. The highest heat transfer coefficient was reached at about 9 m from the step at about 3 w/m^2 K. The Nusselt number for resultant flow after the step was highest at a distance of about 9 m from the step. The coefficient of friction is the dimensionless shear stress of the skin nondimensionalized through dynamic pressure of free stream and the plot showed a decrease with increase in Reynolds number. The temperature plot in Figure 5d shows a decrement with the increasing Reynolds number. The decrement however also decreases with increasing Reynolds number which could lead to an abrupt halt in this behavior at the transition from laminar and turbulent flow and in turbulent flow.

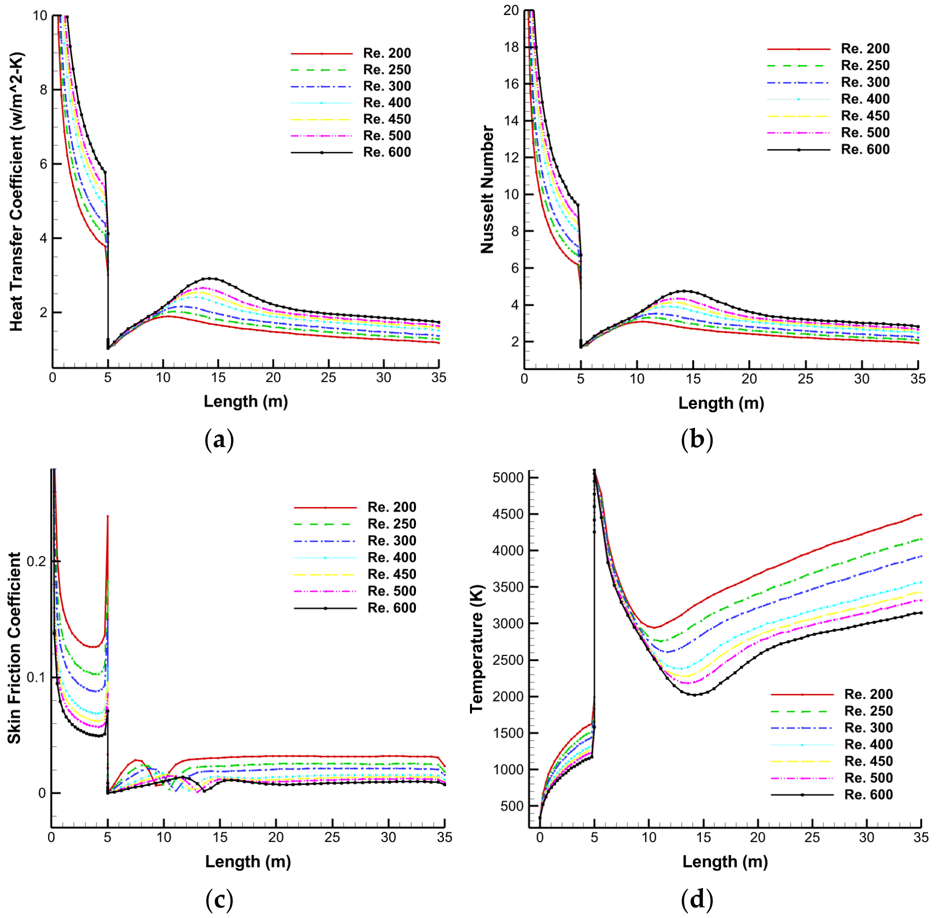

Figure 5. Heat transfer parameters for varying Reynolds numbers: (**a**) heat transfer coefficient, (**b**) Nusselt number, (**c**) skin friction coefficient, and (**d**) temperature.

5.2. Pure Water Flow over Backward Facing Step at ER—3.5

Flow past backward facing step inside a duct with expansion ratio of 3.5 was investigated numerically with a uniform heat flux (UHF) of 5000 W/m^2 and a constant inlet temperature of 303 K. Temperature contours, streamlines, and the heat transfer parameters were reported and analyzed to understand the heat transfer phenomenon at an increased expansion ratio.

Temperature contours for the simulations at an expansion ratio 3.5 are shown in Figure 6. The contours show an increase in temperature with increasing Reynolds number. The temperature was highest along the step wall in lateral direction and the bottom wall near the corner had a higher temperature with decreases along the bottom wall. Since the inlet diameter was smaller than the earlier case, the increased temperature in the current case covered more area when compared. The lateral height of the temperature contours after the reattachment of the resultant flow decreased but it increased after that along the length. At increased velocity of Reynolds number 500 in Figure 6f, the temperature was suppressed from 16 m to about 26 m of the duct's length.

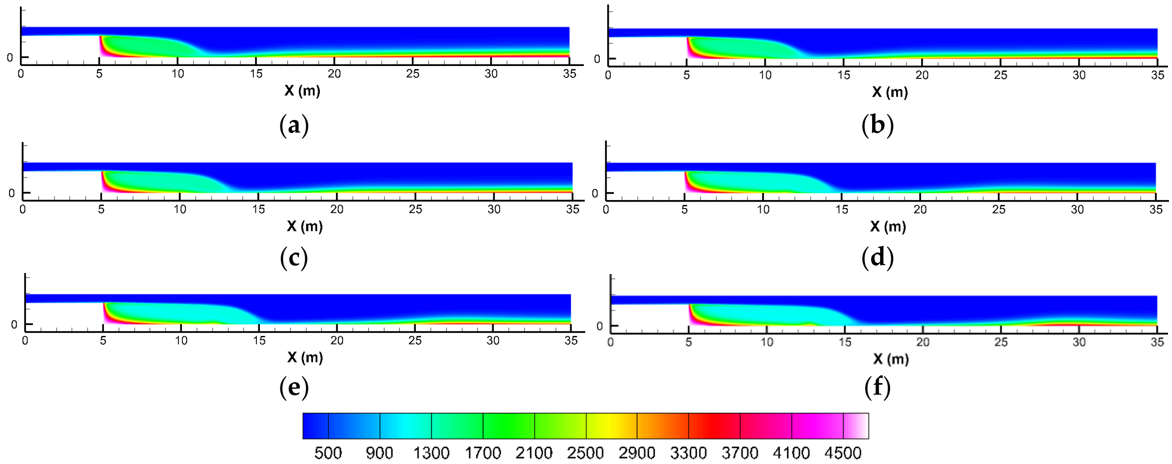

Figure 6. Temperature contours at various Reynolds numbers; (**a**) 200, (**b**) 250, (**c**) 300, (**d**) 400, (**e**) 450, and (**f**) 500.

Streamlines for flow past backward facing step for the expansion ratio 3.5 are shown in Figure 7 for varying Reynolds number. The reattachment length increased for the current case when compared to the expansion ratio of 1.9432. The flow separation occurred at the upper corner at the step and the vortices were formed. Moffatt eddies [2] were at lower corner of the step whose length of the vortex along the longitudinal direction increased. An additional vortex was generated as seen in the current streamlines of the current simulation. Considering Moffatt's research which has described that infinite number of eddies should be expected but they are not generated and shown because lack of reasonable resources, the subsequent eddies are not resolved. For flow past backward facing step, the main important parameters responsible for the flow behavior are the geometry, i.e., expansion ratio and Reynolds numbers. The size of the vortex near the lower corner increased with the increase in Reynolds number. Figure 8 shows the velocity profiles in lateral direction at various lengths from inlet boundary showing the transition of velocity over the backward facing step. Figure 9 shows the length of the recirculation region for a backward facing step having an expansion ratio of 3.5. Figure 10 shows the heat transfer parameters for varying Reynolds number when the ER is 3.5. The heat transfer coefficient was higher for all the Reynolds number when compared to the ER 1.9432. Figure 10d shows that the temperature for higher Reynolds number increased after 25 m from inlet and then again decreased. This phenomenon continued for higher Reynolds numbers and the outlet temperatures for Reynolds numbers 400, 450, and 400 were approximately the same. The Nusselt number for Reynolds number 500 reached its peak at a distance more than 15 m which is higher than the Nusselt number for ER 1.9432 where it reached the peak before 15 m.

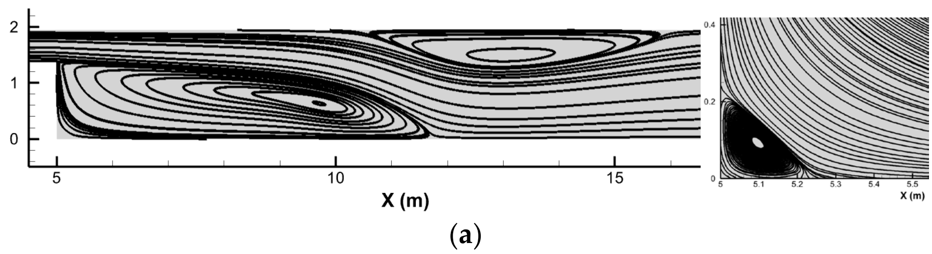

Figure 7. *Cont.*

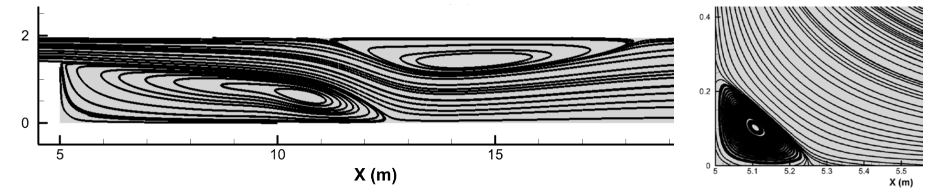

(**b**)

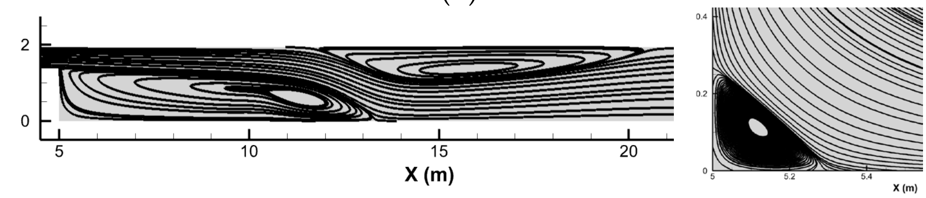

(**c**)

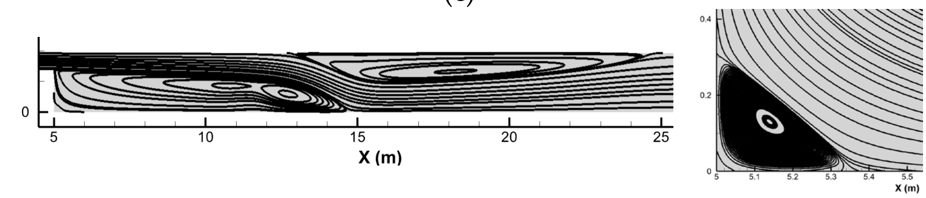

(**d**)

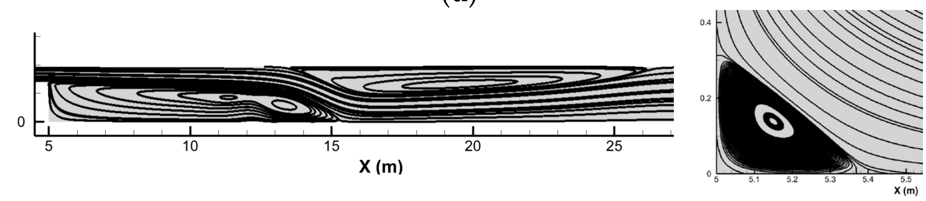

(**e**)

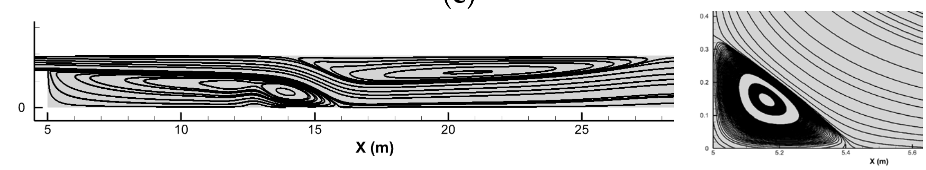

(**f**)

Figure 7. Streamlines various Reynolds numbers; (**a**) 200, (**b**) 250, (**c**) 300, (**d**) 400, (**e**) 450, and (**f**) 500.

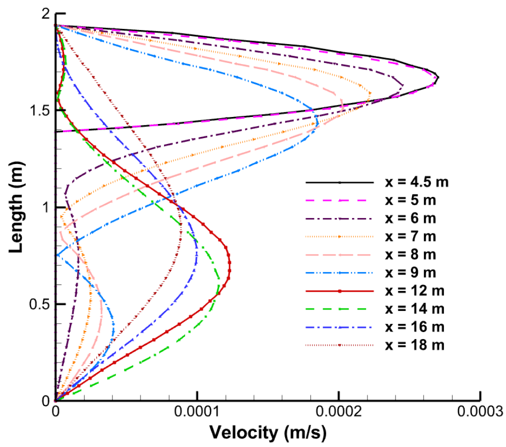

(**a**)

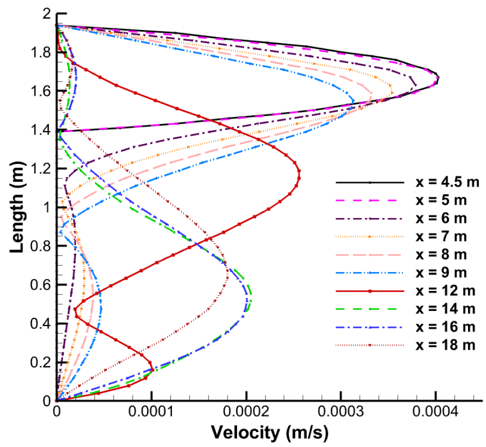

(**b**)

Figure 8. *Cont.*

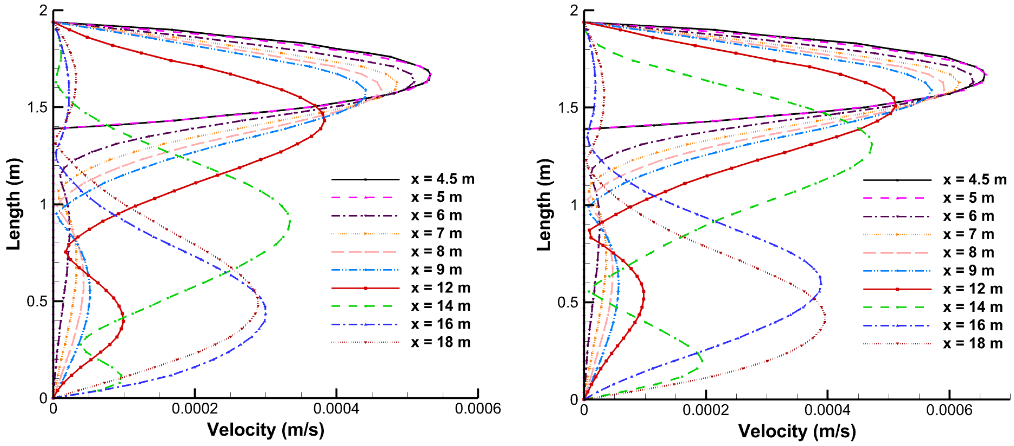

(**c**) (**d**)

Figure 8. Velocity profiles for Reynolds numbers at various lengths along the lateral directions from inlet boundary; (**a**) 200, (**b**) 300, (**c**) 400, and (**d**) 500.

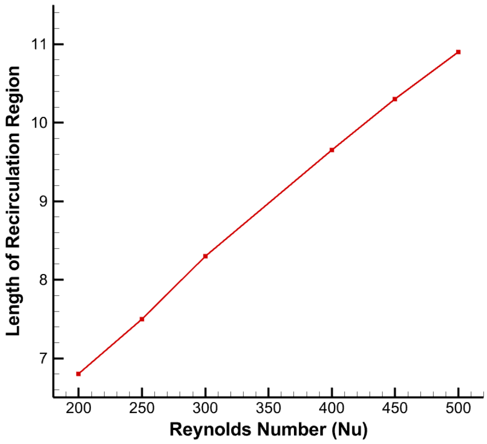

Figure 9. Length of primary recirculation region behind the backward facing step having an expansion ratio of 3.5.

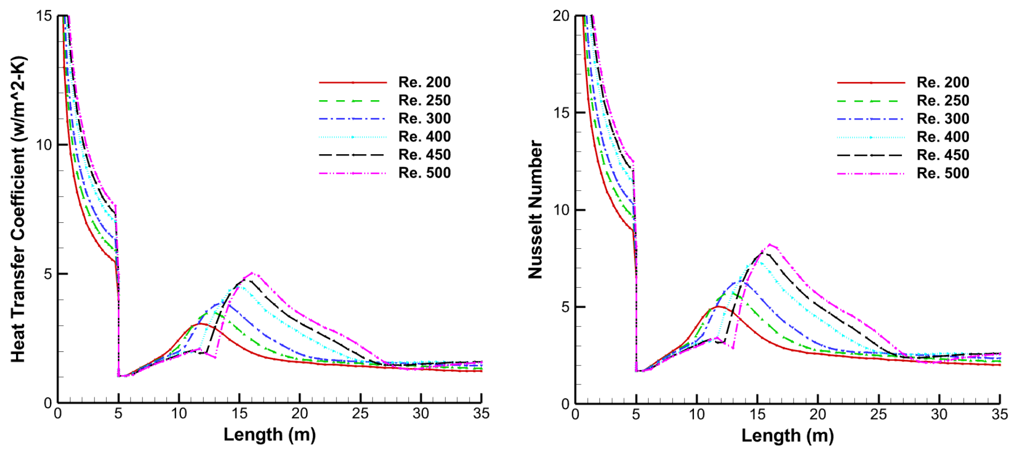

(**a**) (**b**)

Figure 10. *Cont*.

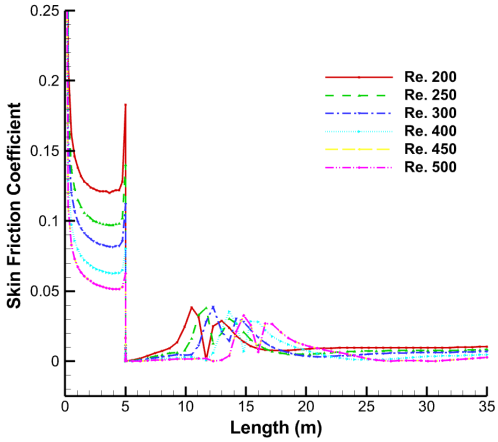

(**c**)

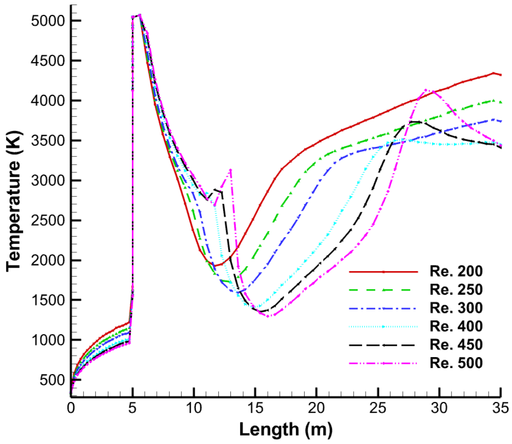

(**d**)

Figure 10. (**a**) Heat transfer coefficient, (**b**) Nusselt number, (**c**) skin friction coefficient, and (**d**) temperature.

5.3. Al_2O_3–H_2O Nanofluid Flow over Backward Facing Step at ER—1.9432

Nanofluid flow over backward facing step at varying Reynolds number was performed. The simulations were performed for volume fractions, $\varphi = 1\%$, 2%, 3%, 4%, and 5% at expansion ratio of 1.9432. Temperature contours were reported and analyzed to understand the change in temperature along the bottom wall. The uniform heat flux (UHF) of 5000 W/m^2 was applied in this case also with inlet temperature kept constant in all the cases as 303 K. The heat transfer was studied by analyzing the coefficient of heat transfer, Nusselt number, coefficient of skin friction, and temperature along the bottom wall.

Figure 11 shows temperature contours for nanofluid flow of 1% volume fraction, over backward facing step inside a duct of expansion ratio 1.9432. The temperature contours showed that the highest temperature at all the Reynolds number were at the vertical wall of step. The flow was separated at the upper corner and the vortices were formed near vertical wall of step thus delaying the reattachment of the flow as shown above in the case of pure water flow over a backward facing step at UHF of 5000 W/m^2. The size of the recirculation region increased with increasing Reynolds number. The temperature, however, was lower along the bottom wall in the longitudinal direction, lower than the case with pure water. Since temperature contours for nanofluid flow showed a lower temperature when compared to pure water flow, outlet temperature for nanofluid flow decreased.

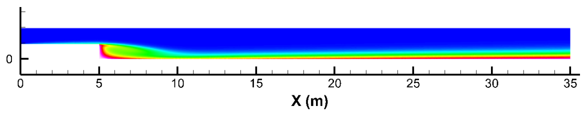

(**a**)

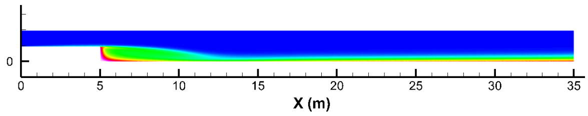

(**b**)

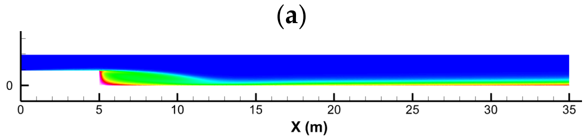

(**c**)

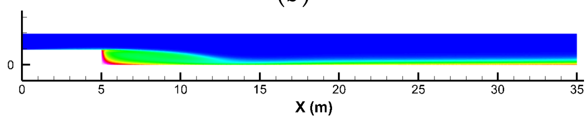

(**d**)

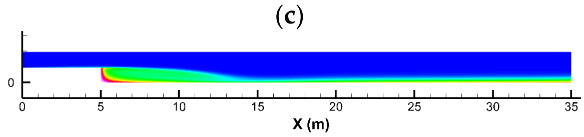

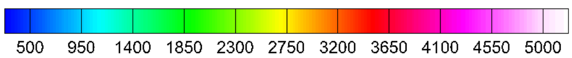

(**e**)

Figure 11. Temperature contours at various Reynolds numbers at volume fraction 1%; (**a**) 200, (**b**) 300, (**c**) 400, (**d**) 500, and (**e**) 600.

Figure 12 shows the resultant coefficient of heat transfer, Nusselt number, coefficient of skin friction, and temperature along the bottom wall. The heat transfer coefficient in Figure 12a is found to increase with increasing Reynolds number. An increased coefficient of heat transfer of the fluid has proven to be a highly effective cooling agents in a various application for various industries. The increment at various Reynolds number shows, there was very little increase at lower Reynolds number compared to at the higher Reynolds number considered. The Nusselt number in Figure 12b increased with the increase in Reynolds number reaching maximum value after the step at about 14.5 m. The coefficient of skin friction in Figure 12c shows that the resultant value decreased on the bottom wall for increasing Reynolds number. The viscosity of the nanofluid defined by the Equation (5) given by [3] increases with increasing volume fraction. The coefficient of skin friction deceased with increasing the inlet flow velocity as shown in Figure 12c. The Reynolds number decided how high the viscosity was with respect to in relation to the inertial forces. A higher Reynolds number resulted in low viscosity which means that the higher Reynolds number almost always results in lower friction. The temperature along the bottom wall is shown in Figure 12d. The plot shows the decrease in temperature with the increase in Reynolds number. The results also show that the outlet temperature has decreased by about 2 °K for all the Reynolds number at 1% volume fraction when compared with the pure water flow. The decrease in temperature was very rapid at lower Reynolds number but it decelerated with increasing Reynolds number. The temperature increased mainly on the wall of step and it started decreasing along bottom wall only to be increased again after the reattachment of the flow.

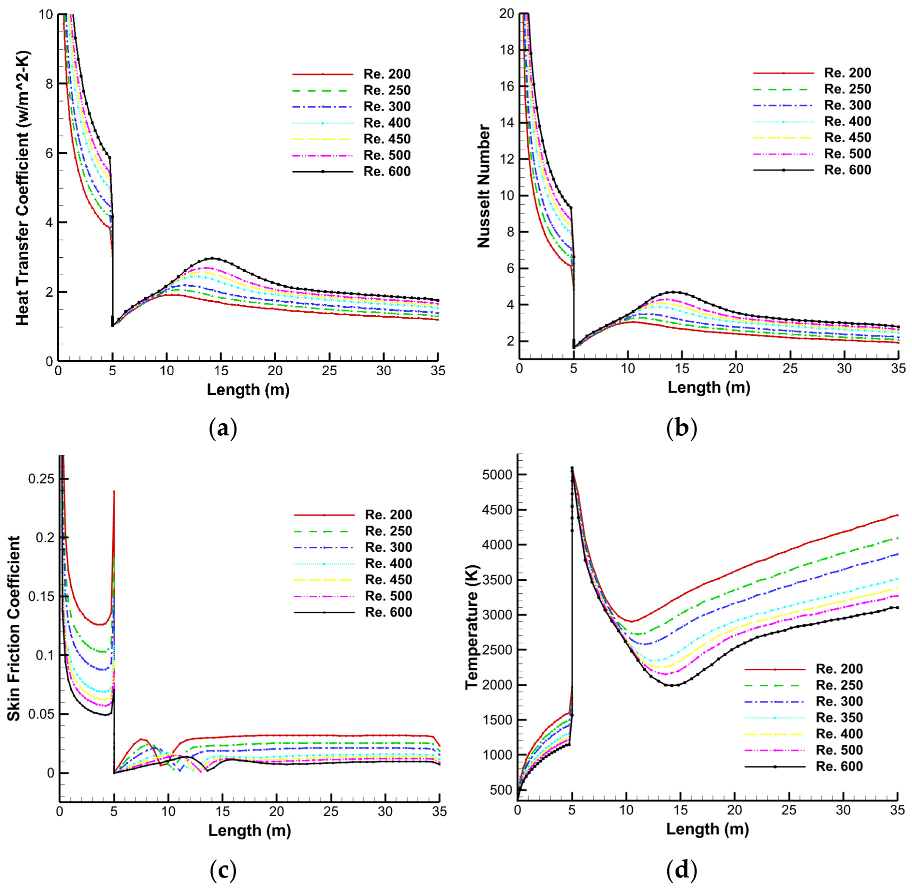

Figure 12. Heat transfer parameters for varying Reynolds numbers for nanofluid at 1% volume fraction (**a**) heat transfer coefficient, (**b**) Nusselt number, (**c**) skin friction coefficient, and (**d**) temperature.

Figure 13 shows the temperature contours for nanofluid flow over the backward facing step for varying Reynolds number at volume fraction 2%. The temperature decreased with increase in volume fraction and the Reynolds number. The location of highest temperature was still at the vertical wall of the step but it decreased after the lower corner of step along the bottom wall in longitudinal direction. The height of temperature distribution in the duct in the lateral direction showed that the temperature in lateral direction decreased at the point of reattachment of the last location of the recirculation zone on the bottom wall in the longitudinal direction. After reattachment point, the temperature again became slightly higher in the lateral direction. In the longitudinal direction, the temperature started increasing after the decrease in temperature after the reattachment location on the bottom wall. With increasing Reynolds number, the temperature decreased on the bottom wall as shown in contours. When comparing with pure water with UHF, the average outlet temperature difference was 4 K.

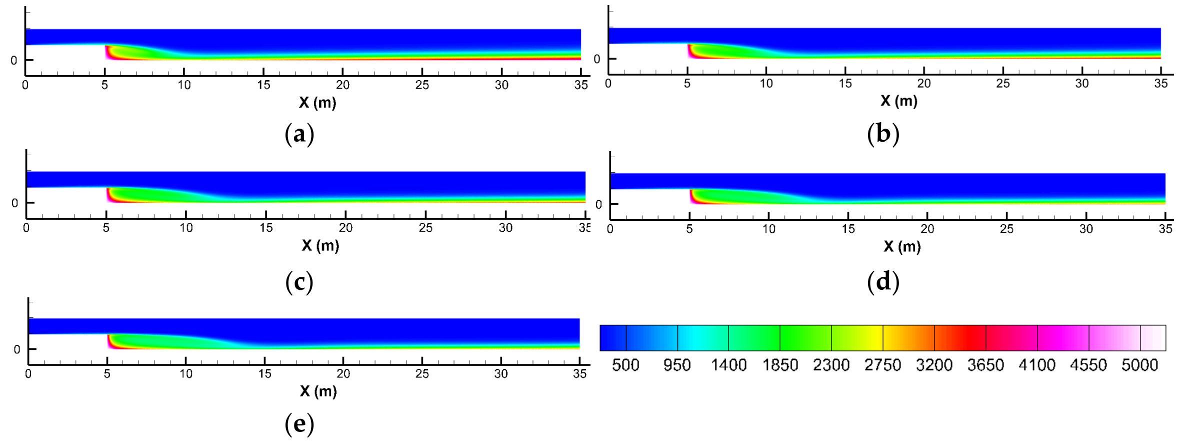

Figure 13. Temperature contours at various Reynolds numbers at volume fraction 2%; (**a**) 200, (**b**) 300, (**c**) 400, (**d**) 500, and (**e**) 600.

The coefficient of heat transfer along bottom wall is depicted in Figure 14a. The plot shows that the value increased with increase in the Reynolds number. The highest value after the step was near the reattachment location on the bottom wall in longitudinal direction. This phenomenon is similar to the above case of nanofluid of volume fraction 1%. The Nusselt number for varying Reynolds numbers is shown in Figure 14b. The Nusselt number increased with the increasing Reynolds number and then it followed a similar trend to the nanofluid of volume fraction 1%. Figure 14c shows the coefficient of skin friction for nanofluid flow of volume fraction of 2%. The resultant values along the bottom wall show a fluctuation between 10–15 m from the inlet and afterwards the fluctuation disappeared and a very slight change in values was observed. The coefficient of skin friction decreased with increase in Reynolds number similar to nanofluid flow of volume fraction 1%. The temperature along the bottom wall followed a similar trend to the previous case. Figures 15 and 16 shows the temperature contours and the heat transfer parameters for the nanofluid flow over the backward facing step at volume fraction 3%. Figures 17 and 18 shows the temperature contours and the heat transfer parameters for the nanofluid flow over the backward facing step at volume fraction 4%. Figures 19 and 20 shows the temperature contours and the heat transfer parameters for the nanofluid flow over the backward facing step at volume fraction 5%. The coefficient of heat transfer increased with an increase in Reynolds number for volume fractions 1–5% as shown in plots and Table 4. The temperature decreased with the increase in Reynolds numbers and volume fraction as shown in Table 5. Since the reattachment length increased with increasing Reynolds number, the area in the duct with higher temperature increased in every case. The temperature, however, decreased with increasing volume fraction. This coefficient of heat transfer increased with volume fraction rate which had the same results as the study of Klazy and Bognar [10]. The values increased for every volume fraction increasing showing an enhancement in heat transfer. The Nusselt number on the bottom wall for volume fraction 3%, 4%, and 5% increased with increase in the Reynolds number.

The coefficient of skin friction decreased with decrease in Reynolds number at volume fractions 3%, 4%, and 5% in Figures 16c, 18c, and 20c. The temperature at the bottom wall for volume fraction 3%, 4%, and 5% at varying Reynolds number are shown in Figures 16d, 18d, and 20d. The temperature decreased for all the volume fractions with increasing Reynolds number. The decrease in average outlet temperature for the three volume fractions 3%, 4%, and 5%, when compared with pure water flow was about 5.2 K, 6 K, and 10 K.

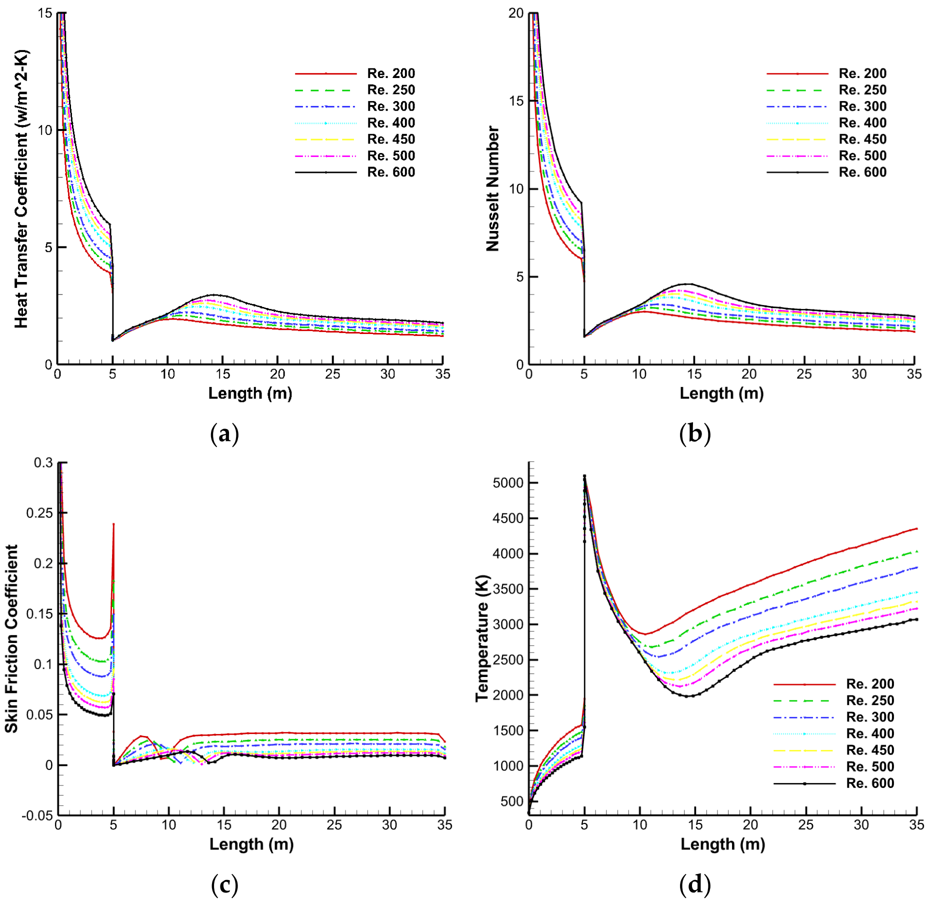

Figure 14. Heat transfer parameters for varying Reynolds numbers for nanofluid at 2% volume fraction; (**a**) heat transfer coefficient, (**b**) Nusselt number, (**c**) skin friction coefficient, and (**d**) temperature.

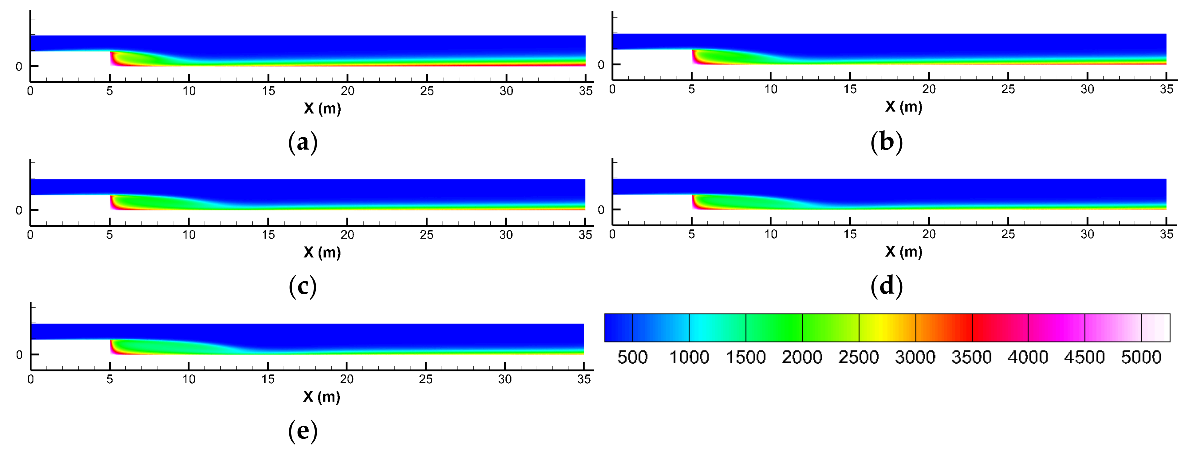

Figure 15. Temperature contours at various Reynolds numbers at volume fraction 3%; (**a**) 200, (**b**) 300, (**c**) 400, (**d**) 500, and (**e**) 600.

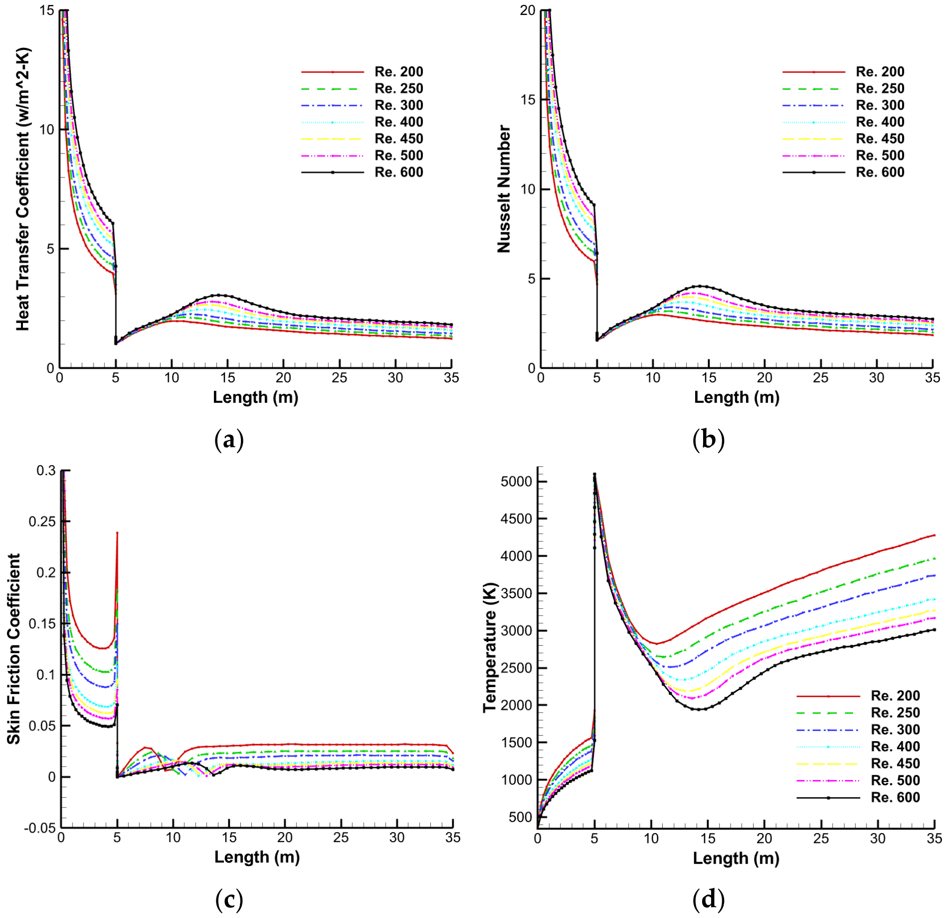

Figure 16. Heat transfer parameters for varying Reynolds numbers for nanofluid at 3% volume fraction; (**a**) Heat transfer coefficient, (**b**) Nusselt number, (**c**) skin friction coefficient, and (**d**) temperature.

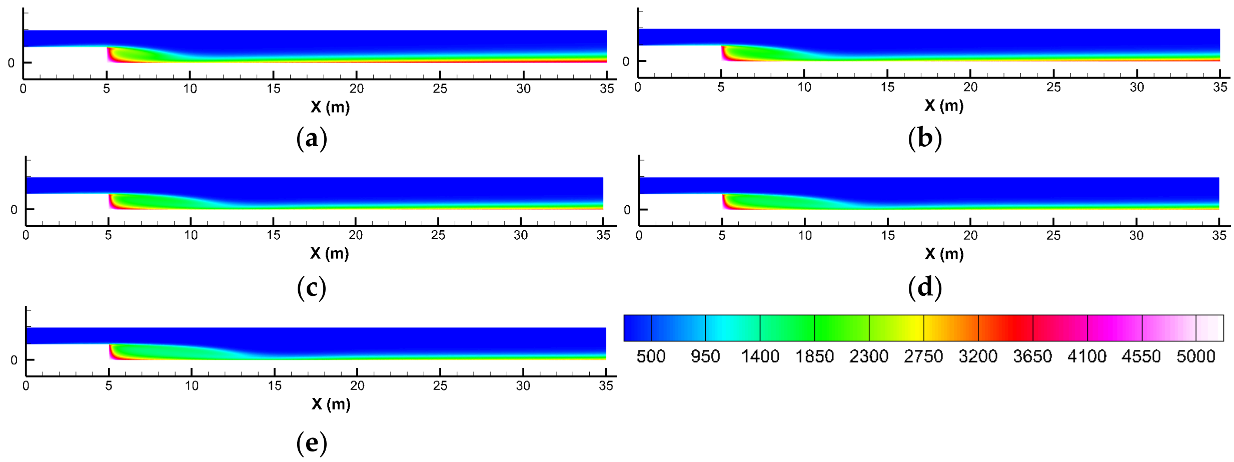

Figure 17. Temperature contours at various Reynolds number at volume fraction 4%; (**a**) 200, (**b**) 300, (**c**) 400, (**d**) 500, and (**e**) 600.

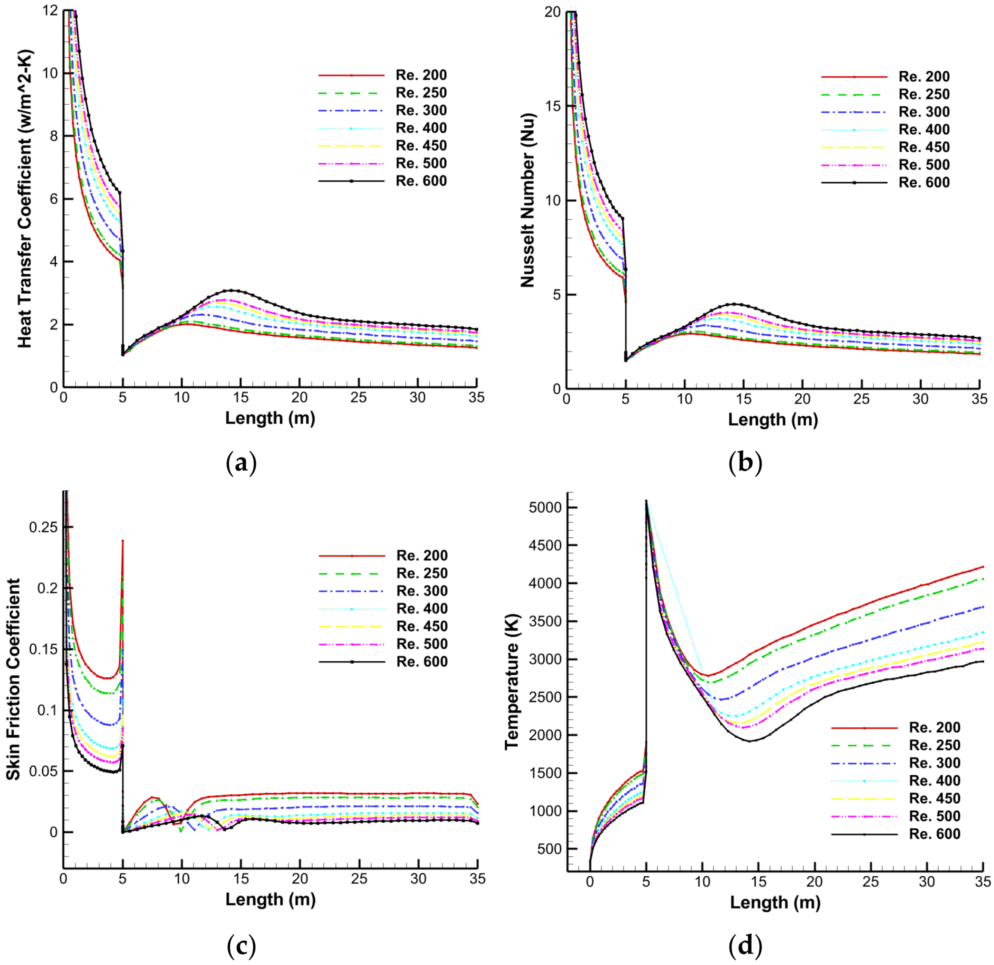

Figure 18. Heat transfer parameters for varying Reynolds number for nanofluid at 4% volume fraction; (**a**) Heat transfer coefficient, (**b**) Nusselt number, (**c**) skin friction coefficient, and (**d**) temperature.

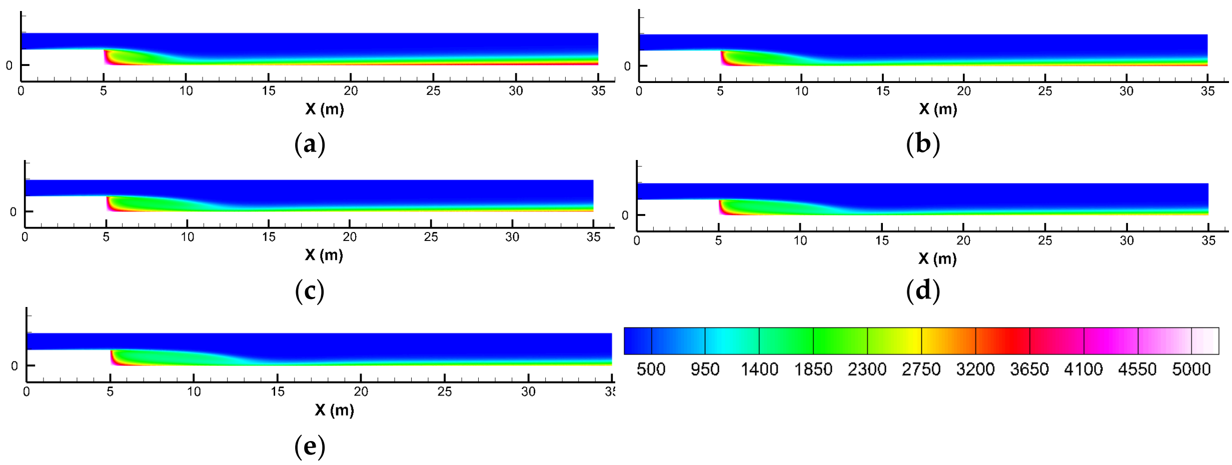

Figure 19. Temperature contours at various Reynolds numbers at volume fraction 5%; (**a**) 200, (**b**) 300, (**c**) 400, (**d**) 500, and (**e**) 600.

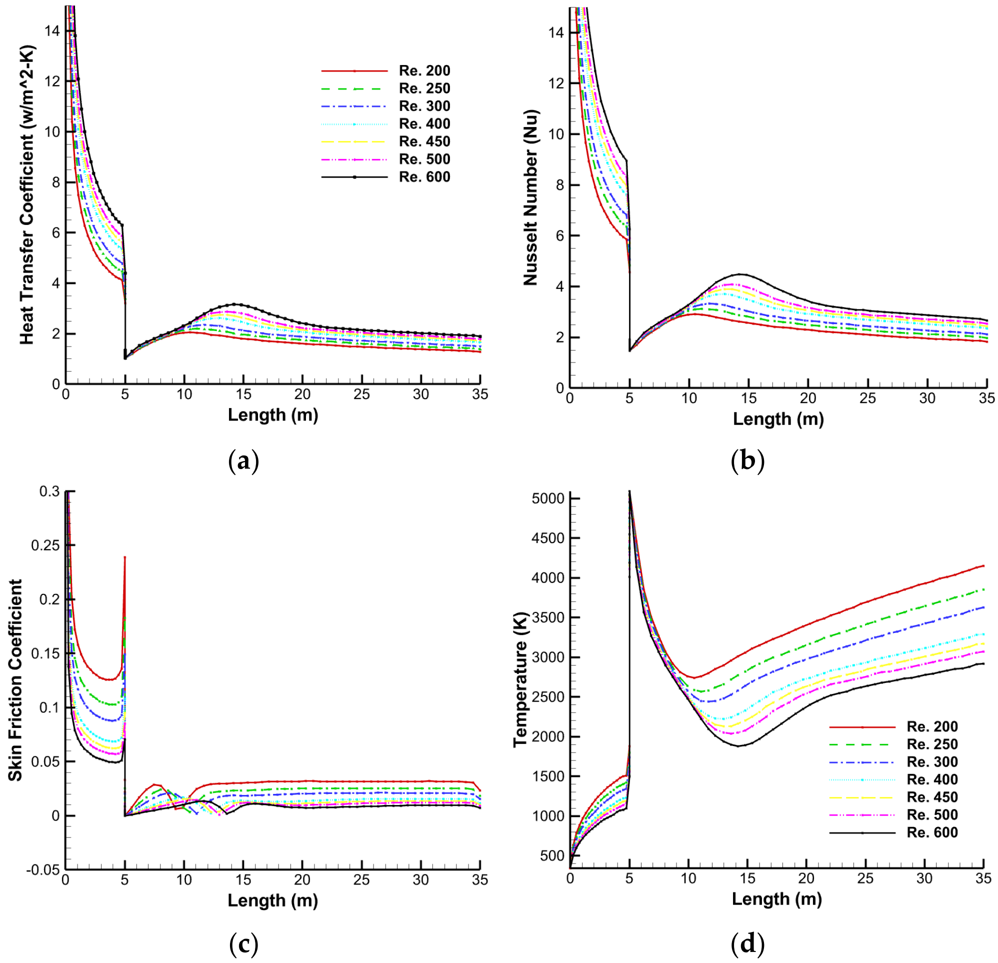

Figure 20. Heat transfer parameters for varying Reynolds numbers for nanofluid at 5% volume fraction; (**a**) heat transfer coefficient, (**b**) Nusselt number, (**c**) skin friction coefficient, and (**d**) temperature.

Table 4. Average coefficient of heat transfer (w/m^2-K) at bottom wall for various Reynolds numbers and volume fractions.

Re.	φ = 0%	φ = 1%	φ = 2%	φ = 3%	φ = 4%	φ = 5%
200	2.676	2.721	2.767	2.814	2.862	2.912
250	2.901	2.948	2.999	3.051	2.981	3.157
300	3.097	3.149	3.204	3.258	3.315	3.373
400	3.439	3.497	3.557	3.599	3.682	3.746
450	3.509	3.653	3.717	3.787	3.847	3.914
500	3.731	3.801	3.866	3.933	3.987	4.072

Table 5. Average outlet temperature for various Reynolds numbers and volume fractions.

Re.	φ = 0%	φ = 1%	φ = 2%	φ = 3%	φ = 4%	φ = 5%
200	985.514	982.999	979.681	996.206	972.392	968.231
250	881.554	879.257	876.299	873.201	921.285	866.314
300	812.561	810.471	807.765	804.961	801.896	798.587
400	715.037	713.241	710.973	713.695	706.055	703.291
450	682.092	680.392	678.264	676.063	673.687	671.161
500	656.011	654.441	652.438	650.346	651.441	645.679

5.4. *Al_2O_3–H_2O Nanofluid Flow over Backward Facing Step at ER—3.5*

Nanofluid flow over backward facing step at varying Reynolds number was performed for an increased expansion ratio of 3.5. The simulations were performed for volume fractions, φ = 1%, 2%, 3%, 4%, and 5%. Temperature contours were analyzed to understand the change in temperature along the bottom wall. The uniform heat flux (UHF) of 5000 W/m^2 was applied in this case also with inlet temperature kept constant in all the cases as 303 K. The heat transfer characteristics were studied by analyzing the coefficient of heat transfer, Nusselt number, coefficient of skin friction, and temperature along the bottom wall.

Nanofluid flow over backward facing step at φ = 1% was investigated and temperature contours are presented in Figure 21. Since the inlet diameter decreased in the current case compared to earlier case of expansion ratio of 1.9432, the flow was more unstable. The length of the reattachment increased as the expansion ration increased. In this case, two-dimensional flow also became unsteady with increasing Reynolds number, but the unsteadiness appeared at lower Reynolds number than the earlier discussed case. The appearance of the vortices on the upper wall also appeared at lower Reynolds number than in the earlier case. The temperature contours showed that the temperature increased after the separation as in the earlier case. The highest temperature was found at the lower corner of step with decreases in both the lateral and longitudinal direction. In Figure 21a, temperature near length of 12 m from inlet decreased in the lateral direction which can be observed as the height of temperature difference. The temperature then increased in lateral height in the longitudinal direction and also along the bottom wall. As the Reynolds number increased, the extent of decreased temperature in the longitudinal direction as in Figure 21f from 15.7 m to about 20 m increased. The temperature after this length increased both in lateral and longitudinal direction. In longitudinal direction along the bottom wall, the temperature decrement from the lower corner was not completely steady. Considering the height of the temperature difference in longitudinal direction, the height of the temperature was observed to decrease in the longitudinal direction. The temperature increased after some distance from the lower corner as between 12.1 m to 13.1 m in Figure 21f. Near the outlet boundary at higher Reynolds number, the temperature decreased slightly in lateral direction which could be observed by decrease in height of the increased temperature spectrum. Table 6 shows the coefficient of heat transfer for various volume fractions at different Reynolds number. The value of coefficient of heat transfer increases with increasing Reynolds number at all the volume fractions 1–5%. The temperature along the bottom wall also decreased near the outlet boundary of the duct with increasing Reynolds number in Table 7. With increase in the Reynolds number, temperature at the outlet boundary decreased. When compared to the pure water, the nanofluid flow exhibited a decrease in temperature at the outlet boundary.

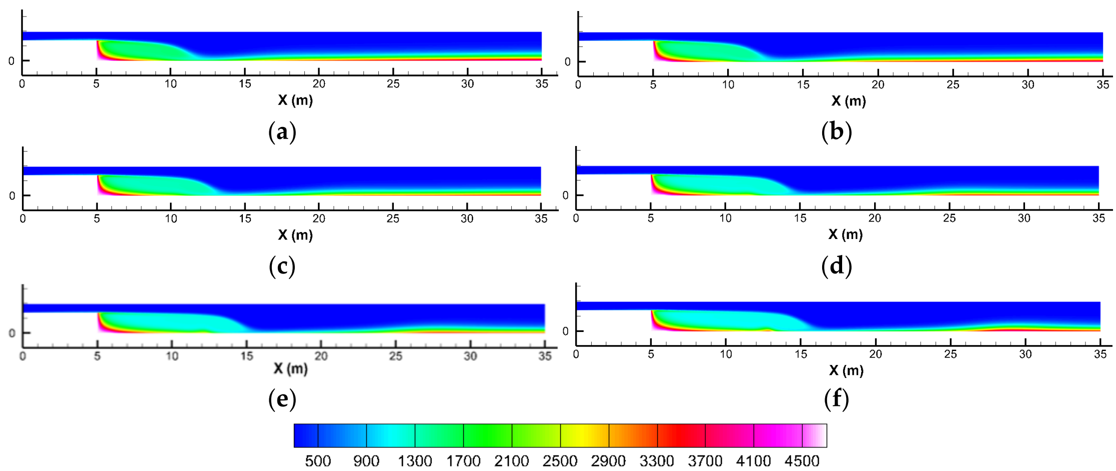

Figure 21. Temperature contours at various Reynolds numbers; (**a**) 200, (**b**) 250, (**c**) 300, (**d**) 400, (**e**) 450, and (**f**) 500.

Figure 22a shows coefficient of heat transfer for φ = 1% along bottom wall for various Reynolds numbers. The coefficient of heat transfer increased with the increase in Reynolds number reaching the highest value between 10–16 m from the inlet boundary in Table 6. The values were also higher when compared with expansion ratio of 1.9432. The plot shows that the value decreased from about 16 m from inlet reaching a minimum value at 28 m for Reynolds number 500 and then started increasing very slowly. Plots for Reynolds number less than 500 did not decrease and reached a minimum as for Reynolds number 500, but became almost constant except for slight changes. Figure 22b shows an increase in Nusselt number for increasing Reynolds number at φ = 1%. The value for Reynolds number 600 decreased after reaching the highest value at about 16 m after the step and reached the minimum at 28 m. The Nusselt number increased very slowly after 28 m but for other Reynolds number, the value decreased and reached the lowest, becoming almost constant with slight changes. The coefficient of skin friction decreased with increase in Reynolds number as shown in Figure 22c. The values fluctuated between 9 and 17 m and then the changes were very small. For higher Reynolds numbers, the values after fluctuation decreased and then increased from 25 m but eventually did not change much. For lower Reynolds numbers, the decrease was much less after the fluctuations and the plot for the Reynolds number had the highest coefficient of skin friction. The temperature on the bottom wall is shown in Figure 22d for φ = 1%.

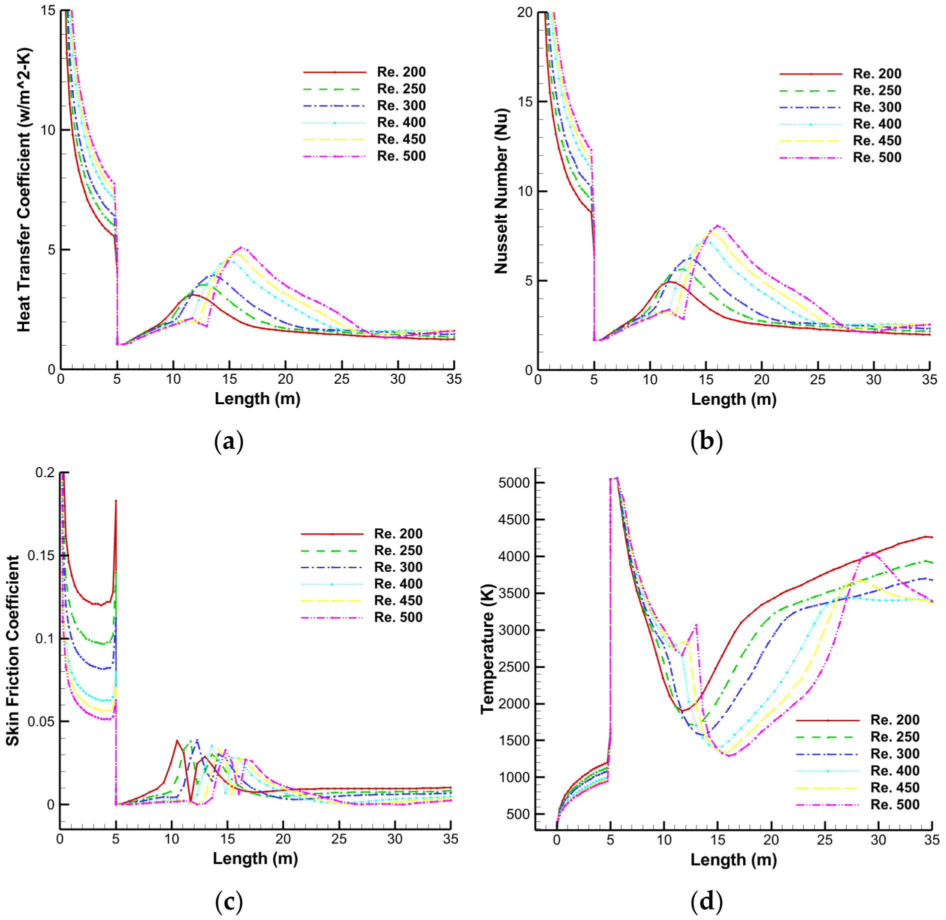

Figure 22. Heat transfer parameters for varying Reynolds numbers for nanofluid at 1% volume fraction; (**a**) heat transfer coefficient, (**b**) Nusselt number, (**c**) skin friction coefficient, and (**d**) temperature.

Figures 23 and 24 shows the temperature contours and the heat transfer parameters for the nanofluid flow over the backward facing step at volume fraction 2%. Figures 25 and 26 shows the temperature contours and the heat transfer parameters for the nanofluid flow over the backward facing step at volume fraction 3%. Figures 27 and 28 shows the temperature contours and the heat transfer parameters for the nanofluid flow over the backward facing step at volume fraction 4%. Figures 29 and 30 shows the temperature contours and the heat transfer parameters for the nanofluid flow over the backward facing step at volume fraction 5%. The coefficient of heat transfer increased with an increase in Reynolds number for volume fractions 1%–5% as shown in plots and Table 7. The Nusselt number is increasing with increasing Reynolds number. The coefficient of heat transfer has also been found to increase with increasing Reynolds number and volume fraction. For the higher Reynolds number, the temperature after the step decreased and then increased with a fluctuation and decreases gain. This phenomenon was not observed for flow at lower Reynolds numbers. The resultant flow at higher Reynolds number also had a fluctuation after the step while decreasing. The current outlet temperature when compared with expansion ratio of 1.9432 was lower for all the Reynolds number. When comparing pure water and nanofluid, the average outlet temperature decreased for all the volume fractions. The flow for expansion ratio 1.9432 showed a vortex at very low Reynolds number when the flow did not separate from top corner of the step. A bigger vortex was created but due to the adverse pressure gradient by a sudden expansion, the edge of the backward facing step induced a separated flow. The flow separation was more prevalent and the flow also became three dimensional when the expansion ratio increased.

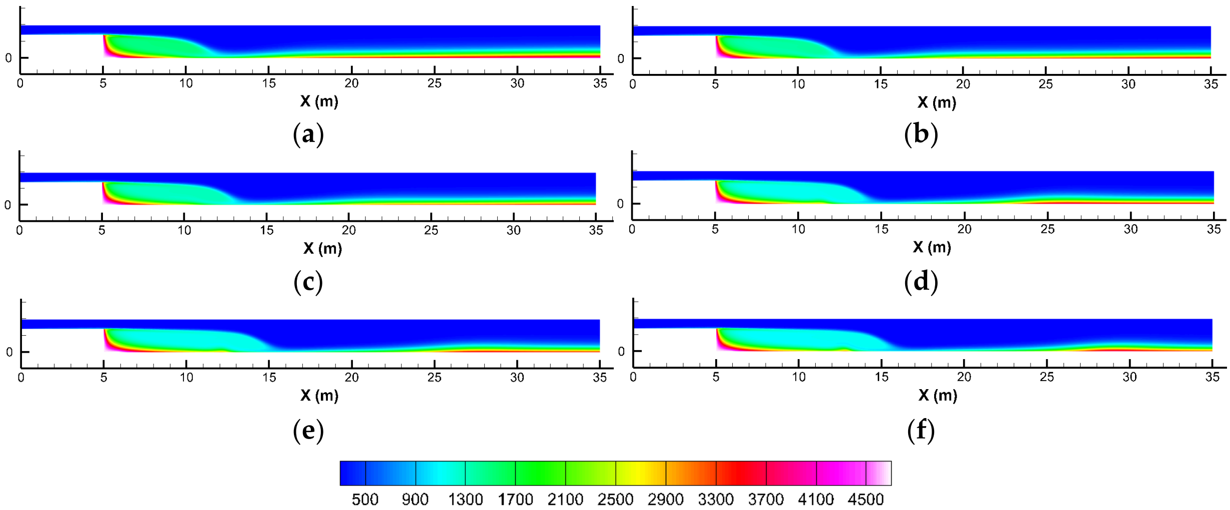

Figure 23. Temperature contours at various Reynolds numbers; (**a**) 200, (**b**) 250, (**c**) 300, (**d**) 400, (**e**) 450, and (**f**) 500.

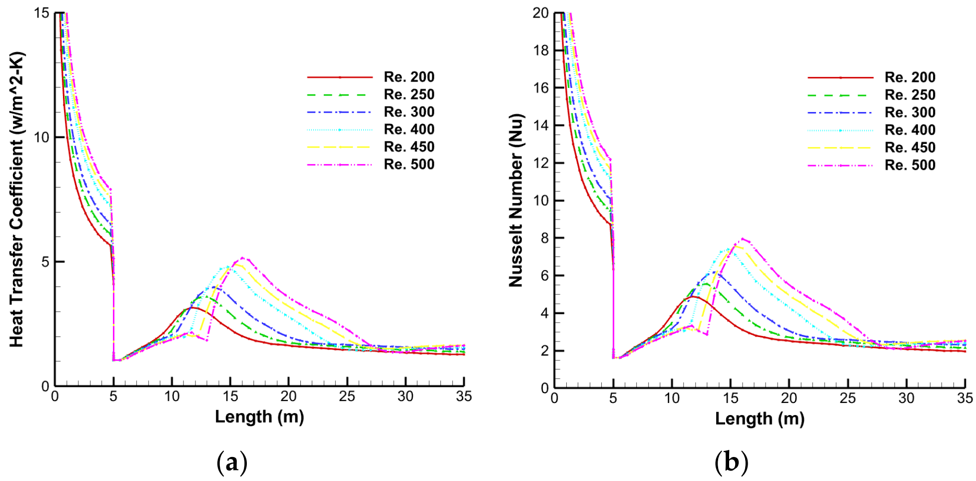

Figure 24. *Cont.*

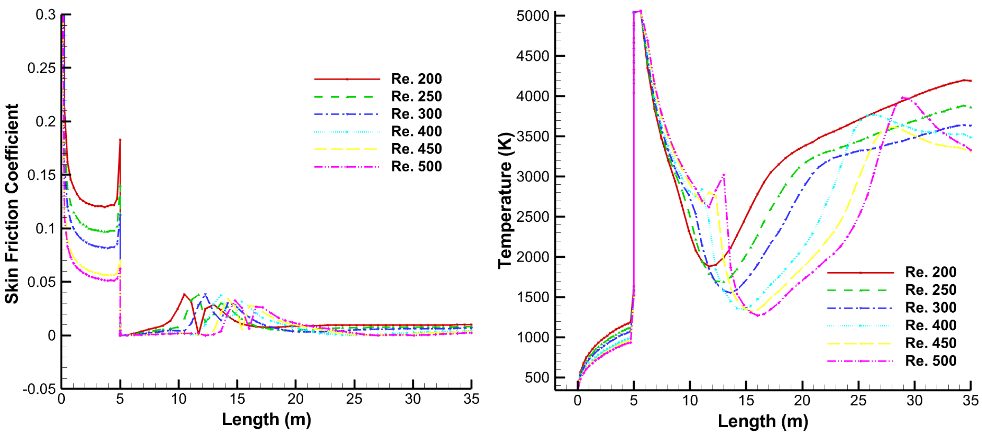

(**c**) (**d**)

Figure 24. Heat transfer parameters for varying Reynolds numbers for nanofluid at 2% volume fraction; (**a**) heat transfer coefficient, (**b**) Nusselt number, (**c**) skin friction coefficient, and (**d**) temperature.

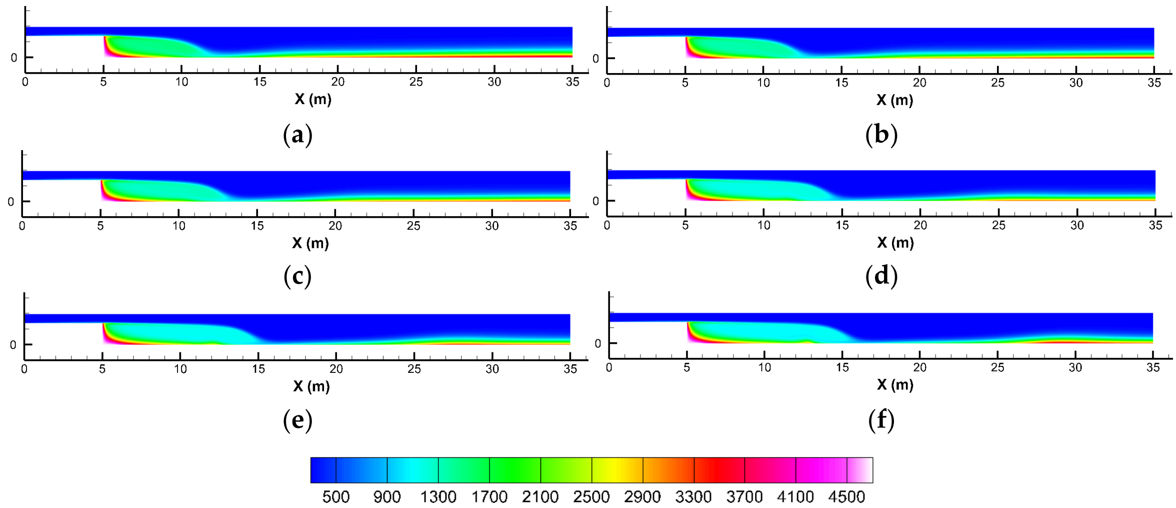

Figure 25. Temperature contours at various Reynolds numbers; (**a**) 200, (**b**) 250, (**c**) 300, (**d**) 400, (**e**) 450, and (**f**) 500.

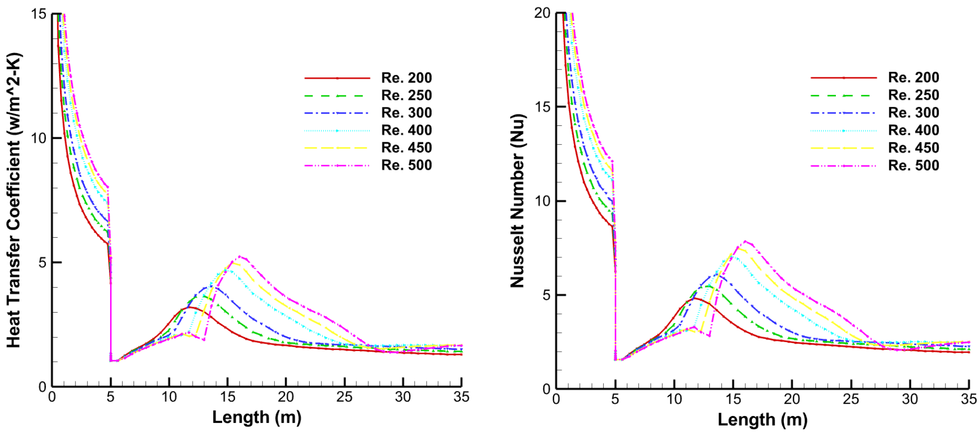

(**a**) (**b**)

Figure 26. *Cont.*

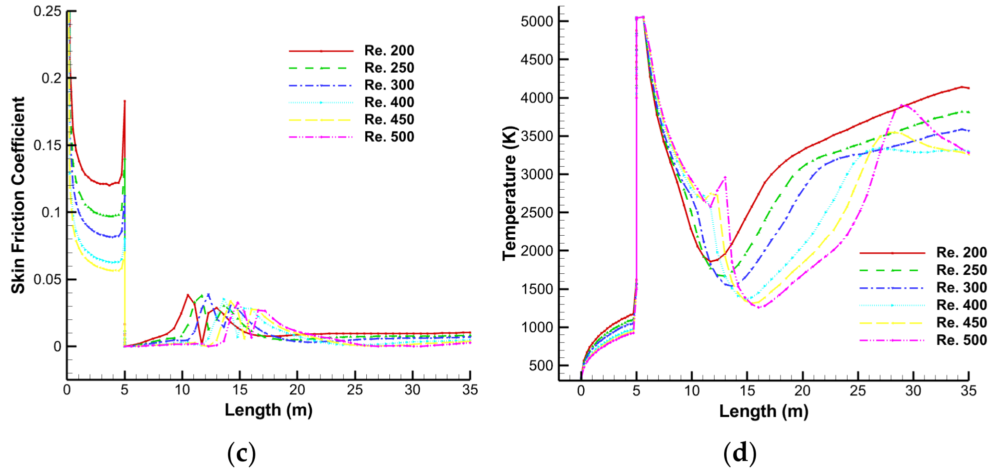

Figure 26. Heat transfer parameters for varying Reynolds numbers for nanofluid at 3% volume fraction; (**a**) heat transfer coefficient, (**b**) Nusselt number, (**c**) skin friction coefficient, and (**d**) temperature.

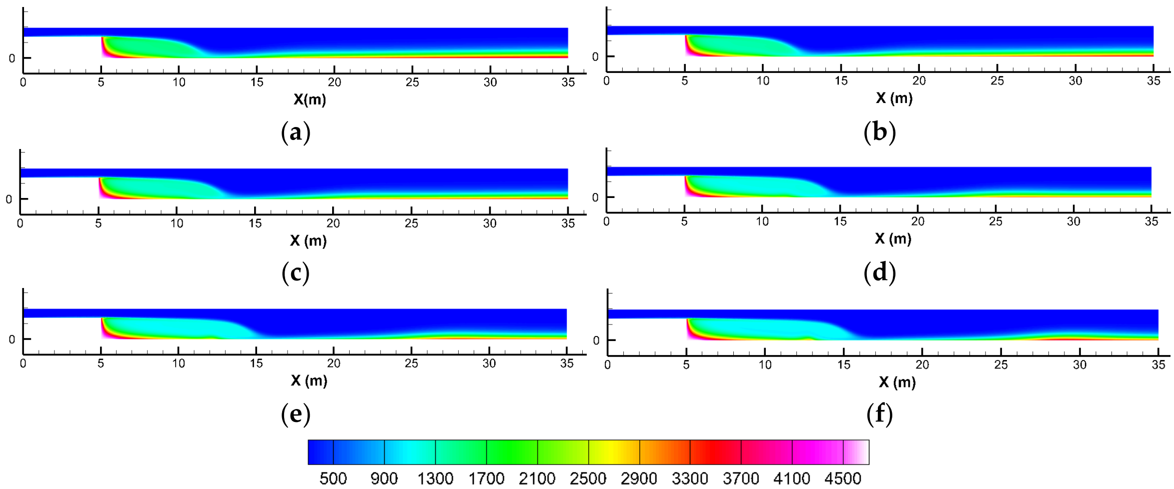

Figure 27. Temperature contours at various Reynolds numbers; (**a**) 200, (**b**) 250, (**c**) 300, (**d**) 400, (**e**) 450, and (**f**) 500.

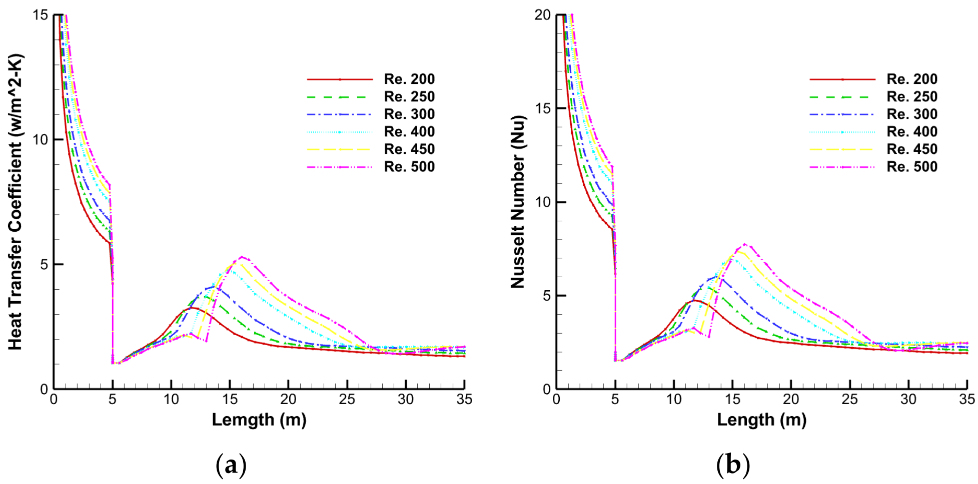

Figure 28. *Cont*.

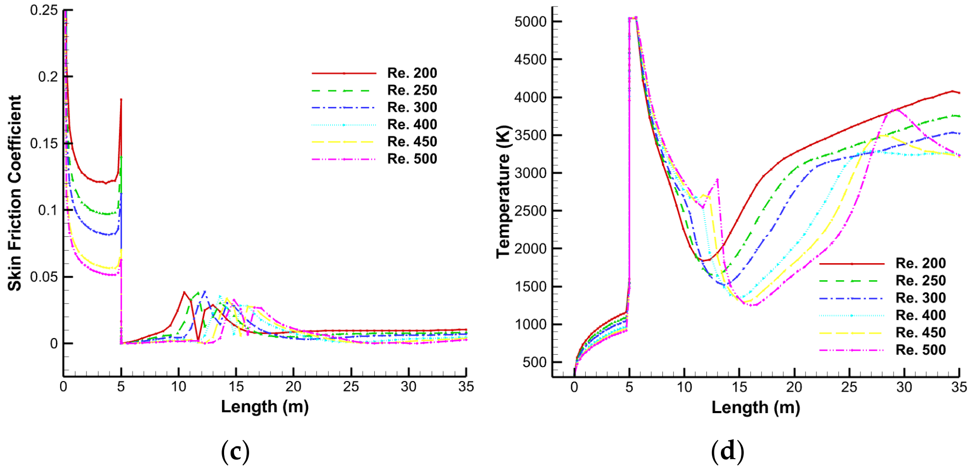

Figure 28. Heat transfer parameters for varying Reynolds numbers for nanofluid at 4% volume fraction; (**a**) heat transfer coefficient, (**b**) Nusselt number, (**c**) skin friction coefficient, and (**d**) temperature.

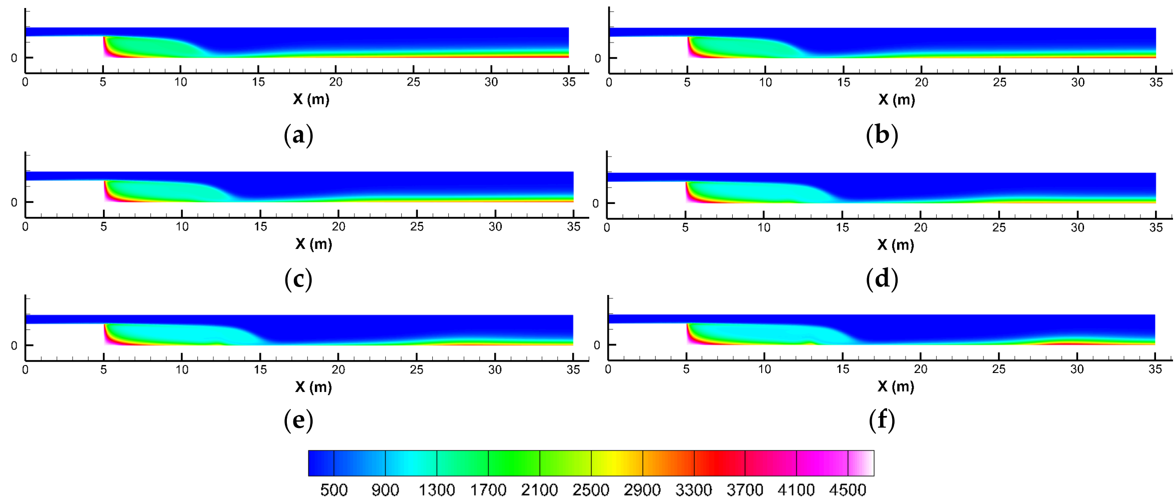

Figure 29. Temperature contours at various Reynolds numbers; (**a**) 200, (**b**) 250, (**c**) 300, (**d**) 400, (**e**) 450, and (**f**) 500.

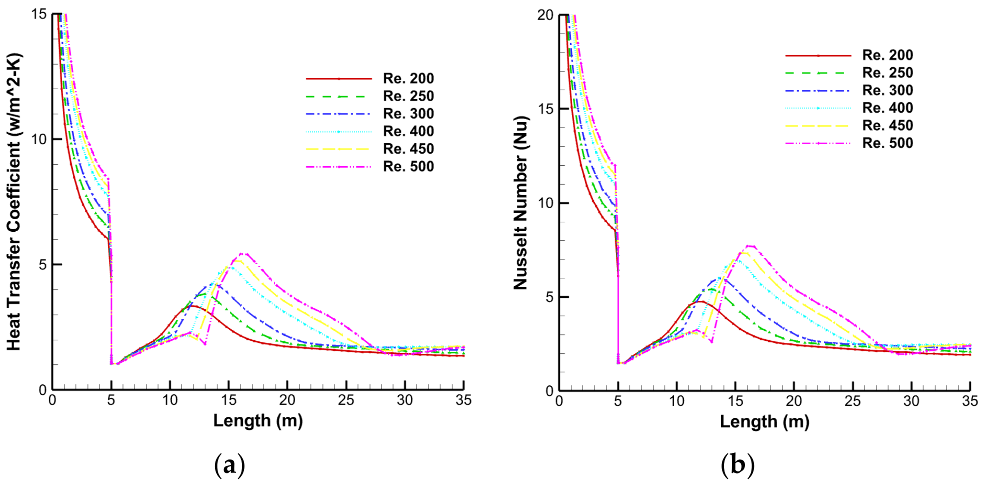

Figure 30. *Cont.*

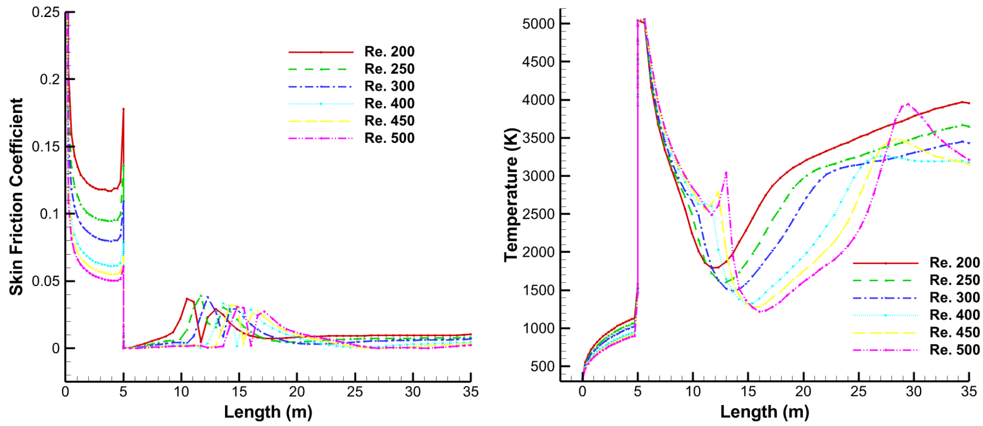

(**c**) (**d**)

Figure 30. Heat transfer parameters for varying Reynolds numbers for nanofluid at 5% volume fraction; (**a**) heat transfer coefficient, (**b**) Nusselt number, (**c**) skin friction coefficient, and (**d**) temperature.

Table 6. Average coefficient of heat transfer (w/m^2-K) at bottom wall for various Reynolds numbers and volume fractions.

Re.	φ = 0%	φ = 1%	φ = 2%	φ = 3%	φ = 4%	φ = 5%
200	2.822	2.868	2.915	2.964	3.014	3.096
250	3.071	3.121	3.172	3.225	3.279	3.369
300	3.288	3.341	3.397	3.454	3.512	3.607
400	3.651	3.711	3.751	3.836	3.901	4.006
450	3.801	3.863	3.928	3.994	4.062	4.171
500	3.938	4.003	4.071	4.139	4.211	4.319

Table 7. Average outlet temperature for various Reynolds numbers and volume fractions.

Re.	φ = 0%	φ = 1%	φ = 2%	φ = 3%	φ = 4%	φ = 5%
200	982.637	980.281	977.138	973.812	970.170	952.937
250	875.913	873.799	871.005	868.101	864.911	850.448
300	803.036	801.078	798.547	795.912	793.051	780.773
400	722.028	720.151	747.907	715.423	712.793	705.128
450	709.257	707.209	704.747	702.305	699.578	694.095
500	715.197	712.908	710.112	707.211	704.291	710.633

6. Conclusions

Nanofluid flow over a backward facing step placed in a duct was numerically investigated to determine the heat transfer characteristics for a single-phase model. Numerical simulation was performed for two expansion ratios at various Reynolds numbers in laminar flow regime considering volume fractions φ = 1%, 2%, 3%, 4%, and 5%. The model was validated with the existing literature and the current results agree with results from existing literature. The results of the paper are as follows:

1. The coefficient of heat transfer increased with increasing Reynolds number and the volume fraction for both the expansion ratios.
2. The Nusselt number increased with the increasing Reynolds number for all investigated volume fractions for both expansion ratios.
3. The coefficient of skin friction decreased with the increasing Reynolds number and volume fraction in both the expansion ratios.
4. A higher coefficient of heat transfer and Nusselt number was observed for geometry having a higher expansion ratio.

5. The temperature on the bottom wall also decreased with increasing Reynolds number at varying volume fractions in both expansion ratios.
6. The coefficient of heat transfer at φ = 5% was higher by 63.11% and 9.66% than the pure water for ER = 1.9432 and ER = 3.5. At φ = 5%, the outlet temperature for the duct decreased by 10 °K and 5 °K when compared to the pure water for ER = 1.9432 and ER = 3.5.

The flow being laminar allowed conduction far better than convection. The coefficient of heat transfer was found to increase with increasing the nanoparticle volume fraction. The increase in velocity led to increment in Nusselt number for all the volume fractions investigated. The outlet temperature decreased for all the volume fractions as the Reynolds number increased. A similar phenomenon was observed for both the expansion ratios and for the second case, that of expansion ratio 3.5, the streamlines and contours showed a much more unstable flow after the flow passed over the backward facing step when compared to the case having an expansion ratio 1.9432. The temperature at the outlet also varied as the inlet diameter became lower.

A forward facing step would have a more complex field because of the separation and recirculation zone. Not a lot of research has been performed for the flow over a forward facing step to understand the heat transfer characteristics. Numerical simulations and experimental analysis could help in further understanding the heat transfer characters and flow phenomena. A three-dimensional analysis would help in understanding the nature of flow phenomena at higher Reynolds numbers. A very fine mesh with high-end resources would help in studying Moffatt eddies. Investigation at higher Reynolds numbers during flow transitions from laminar to the turbulent regime would help in understanding the heat transfer characteristics of the nanofluid in the transition regime.

Author Contributions: Conceptualization, W.-C.W. and A.K.; methodology, W.-C.W. and A.K.; validation, W.-C.W. and A.K.; formal analysis, W.-C.W. and A.K.; investigation, W.-C.W. and A.K.; data curation, W.-C.W. and A.K.; writing—original draft preparation, W.-C.W. and A.K.; writing—review and editing, W.-C.W. and A.K.; visualization, W.-C.W. and A.K.; supervision, W.-C.W.; project administration, W.-C.W. All authors have read and agreed to the published version of the manuscript.

Funding: This work was support by the Ministry of Education the Republic of China under Grand Contract PEE1101037.

Conflicts of Interest: The authors declare no conflict of interest.

Abbreviations

Re	Reynolds number
Nu	Nusselt number
E.R.	Expansion ratio
UHF	Uniform heat flux

Nomenclature

φ	Volume fraction
μ	Viscosity
k	Thermal conductivity
c_p	Specific heat
D	Height of the duct
d	Height of the inlet
F_b	Body force term
F_s	Source term
h	Coefficient of heat transfer
K	Kelvin
T	Temperature
u	Velocity in x direction
v	Velocity in y direction

Subscripts

f	Base fluid
nf	Nanofluid
p	Nanoparticle
avg	Average

References

1. Choi, S.U.S. Nanofluids: From Vision to Reality through Research. *J. Heat Transf.* **2009**, *131*, 033106. [CrossRef]
2. Moffatt, H.K. Viscous and resistive eddies near a sharp corner. *J. Fluid Mech.* **1964**, *18*, 1–18. [CrossRef]
3. Roache, P.J. *Computational Fluid Dynamics*; Hermosa Publishers: Socorro, NM, USA, 1972; pp. 139–173.
4. Durst, F.; Peireira, J.C.F. Time-dependent laminar backward facing step flow in a two-dimensional duct. *ASME J. Fluids Eng.* **1988**, *110*, 289–296. [CrossRef]
5. Taylor, T.D.; Ndefo, E. Computation of viscous flow in a channel by the method of splitting. In Proceedings of the Second International Conference on Numerical Methods in Fluid Dynamics, Lecture Notes in Physics, Berkeley, CA, USA, 15–19 September 1970; Volume 8. [CrossRef]
6. Armaly, B.F.; Durst, F.; Pereira, J.C.F.; Schönung, B. Experimental and theoretical investigation of backward-facing step flow. *J. Fluid Mech.* **1983**, *127*, 473–496. [CrossRef]
7. Biswas, G.; Breuer, M.; Durst, F. Backward-Facing Step Flows for Various Expansion Ratios at Low and Moderate Reynolds Numbers. *J. Fluids Eng.* **2004**, *126*, 362–374. [CrossRef]
8. Abedalh, A.S.; Shaalan, Z.A.; Yassien, H.N.S. Mixed convective of hybrid nanofluids flow in a backward facing step. *Case Stud. Therm. Eng.* **2021**, *25*, 100868. [CrossRef]
9. Abdulrazzaq, T.; Togun, H.; Alsulami, H.; Goodarzi, M.; Safaei, M.R. Heat Transfer Improvement in a Double Backward-Facing Expanding Channel Using Different Working Fluids. *Symmetry* **2020**, *12*, 1088. [CrossRef]
10. Klazly, M.; Bognar, G. Heat transfer enhancement for nanofluid flows over a microscale backward-facing step. *Alex. Eng. J.* **2022**, *61*, 8161–8176. [CrossRef]
11. Klazly, M.; Mahabaleshwar, U.S.; Bognar, G. Comparison of single-phase Newtonian and non-Newtonian nanofluid and two-phase models for convective heat transfer of nanofluid flow in backward-facing step. *J. Mol. Liq.* **2022**, *361*, 119607. [CrossRef]
12. Safaei, M.R.; Elkotb, M.A.; Alsharif, A.M.; Mansir, I.B.; Alamri, S.; Tirth, V.; Goodarzi, M. An innovative design of a high strength and low weight sudden micro expansion by considering a nanofluid: Electronic cooling application. *Case Stud. Therm. Eng.* **2021**, *28*, 101637. [CrossRef]
13. Goldanlou, A.S.; Badri, M.; Heidarshenas, B.; Hussein, A.K.; Rostami, S.; Shadloo, M.S. Numerical Investigation on Forced Hybrid Nanofluid Flow and Heat Transfer Inside a Three-Dimensional Annulus Equipped with Hot and Cold Rods: Using Symmetry Simulation. *Symmetry* **2020**, *12*, 11. [CrossRef]
14. Hilo, A.K.; Talib, A.R.A.; Iborra, A.A.; Sultan, M.T.H.; Hamid, M.F. A, Experimental study of nanofluids flow and heat transfer over a backward-facing step channel. *Powder Technol.* **2020**, *372*, 497–505. [CrossRef]
15. Moosavi, R.; Moltafet, R.; Lin, C.-X.; Chuang, P.-Y.A. Numerical modeling of fractional viscoelastic non-Newtonian fluids over a backward facing step–Buoyancy driven flow and heat transfer. *Therm. Sci. Eng. Prog.* **2021**, *21*, 100767. [CrossRef]
16. Careglio, C.; Canales, C.; Papeleux, L.; Ponthot, J.-P.; Garino, C.G.G.; Mirasso, A.E. An implementation of the generalized Maxwell viscoelastic constitutive model. *Mećanica Comput.* **2014**, *33*, 1179–1192.
17. Renaud, F.; Dion, J.-L.; Chevallier, G.; Tawfiq, I.; Lemaire, R. A new identification method of viscoelastic behavior: Application to the generalized Maxwell model. *Mech. Syst. Sig. Process.* **2011**, *25*, 991–1010. [CrossRef]
18. Hayat, T.; Nadeem, S.; Asghar, S. Periodic unidirectional flows of a viscoelastic fluid with the fractional Maxwell model. *Appl. Math. Comput.* **2004**, *151*, 153–161. [CrossRef]
19. Lund, L.A.; Omar, Z.; Dero, S.; Chu, Y.; Khan, I.; Nisar, K.S. Temporal stability analysis of magnetized hybrid nanofluid propagating through an unsteady shrinking sheet: Partial slip conditions. *Comput. Mater. Contin.* **2021**, *66*, 1963–1975.
20. Kolsi, L.; Selimendigil, F.; Said, L.B.; Mesloub, A.; Alresheedi, F. Forced Convection of Non-Newtonian Nanofluid Flow over a Backward Facing Step with Simultaneous Effects of Using Double Rotating Cylinders and Inclined Magnetic Field. *Mathematics* **2021**, *9*, 23. [CrossRef]
21. Abbas Nadeem Nadeem, S.; Saleem Anber Malik, M.Y.; Issakhov, A.; Alharbi, F.M. Models base study of inclined MHD of hybrid nanofluid flow over nonlinear stretching cylinder. *Chin. J. Phys.* **2021**, *69*, 109–117. [CrossRef]
22. Kumar, R.N.; Gowda, R.J.P.; Abusorrah, A.M.; Mahrous, Y.M.; Abu-Hamdeh, N.H.; Issakhov, A.; Rahimi-Gorji, M.; Kumar, B.C. Prasanna, Impact of magnetic dipole on ferromagnetic hybrid nanofluid flow over a stretching cylinder. *Phys. Scr.* **2021**, *96*, 4. [CrossRef]
23. Paul, A.; Das, T.K.; Nath, J.M. Numerical investigation on the thermal transportation of MHD Cu/Al2 O3-H2O Casson-hybrid-nanofluid flow across an exponentially stretching cylinder incorporating heat source. *Phys. Scr.* **2022**, *97*, 8. [CrossRef]
24. Maskeen, M.M.; Zeeshan, A.; Mehmood, O.U.; Hassan, M. Heat transfer enhancement in hydromagnetic alumina–copper/water hybrid nanofluid flow over a stretching cylinder. *J. Therm. Anal. Calorim.* **2019**, *138*, 1127–1136. [CrossRef]

25. Khashi, N.S.; Waini, I.; Zainal, N.A.; Hamzah, K.; Kasim, A.R.M. Hybrid Nanofluid Flow Past a Shrinking Cylinder with Prescribed Surface Heat Flux. *Symmetry* **2020**, *12*, 9. [CrossRef]
26. John Christopher, A.; Magesh, N.; Punith Gowda, R.J.; Naveen Kumar, R.; Varun Kumar, R.S. Hybrid nanofluid flow over a stretched cylinder with the impact of homogeneous–heterogeneous reactions and Cattaneo–Christov heat flux: Series solution and numerical simulation. *Heat Transf. Wiley* **2021**, *50*, 3800–3821. [CrossRef]
27. Sreedevi, P.; Reddy, P.S. Williamson hybrid nanofluid flow over swirling cylinder with Cattaneo–Christov heat flux and gyrotactic microorganism. In *Waves Random Complex Media*; Taylor & Francis: London, UK, 2021; pp. 1–28. [CrossRef]
28. Jabbaripour, B.; Nademi Rostami, M.; Dinarvand, S.; Pop, I. Aqueous aluminium–copper hybrid nanofluid flow past a sinusoidal cylinder considering three-dimensional magnetic field and slip boundary condition. *Proc. Inst. Mech. Eng. Part E J. Process Mech. Eng.* **2021**. [CrossRef]
29. Rajesh, V.; Chamkha, A.; Kavitha, M. Numerical investigation of Ag-CuO/water hybrid nanofluid flow past a moving oscillating cylinder with heat transfer. *Math. Methods Appl. Sci.* **2020**. [CrossRef]
30. Suleman, M.; Ramzan, M.; Ahmad, S.; Lu, D. Numerical simulation for homogeneous—heterogeneous reactions and Newtonian heating in the silver-water nanofluid flow past a nonlinear stretched cylinder. *Phys. Scr.* **2019**, *94*, 085702. [CrossRef]
31. Patil, P.M.; Kulkarni, M. Analysis of MHD mixed convection in a Ag-TiO2 hybrid nanofluid flow past a slender cylinder. *Chin. J. Phys.* **2021**, *73*, 406–419. [CrossRef]
32. Grosan, T.; Pop, I. Axisymmetric mixed convection boundary layer flow past a vertical cylinder in a nanofluid. *Int. J. Heat Mass Transf.* **2011**, *54*, 3139–3145. [CrossRef]
33. Sarkar, S.; Ganguly, S.; Dalal, A.; Saha, P.; Chakraborty, S. Mixed convective flow stability of nanofluids past a square cylinder by dynamic mode decomposition. *Int. J. Heat Fluid Flow* **2013**, *44*, 624–634. [CrossRef]
34. Arjun, K.S.; Rakesh, K. Heat transfer in magnetohydrodynamic nanofluid flow past a circular cylinder. *Phys. Fluids* **2020**, *32*, 045112. [CrossRef]
35. Singh, K.; Pandey, A.K.; Kumar, M. Melting heat transfer assessment on magnetic nanofluid flow past a porous stretching cylinder. *J. Egypt. Math. Soc.* **2021**, *29*, 1. [CrossRef]
36. Mishra, A.; Kumar, M. Velocity and thermal slip efects on MHD nanofuid fow past a stretching cylinder with viscous dissipation and Joule heating. *SN Appl. Sci.* **2020**, *2*, 1350. [CrossRef]
37. Selvakumar, R.D.; Dhinakaran, S. Nanofluid flow and heat transfer around a circular cylinder: A study on effects of uncertainties in effective properties. *J. Mol. Liq.* **2016**, *223*, 572–588. [CrossRef]
38. Pandey, A.K.; Kumar, M. Boundary layer flow and heat transfer analysis on Cu-water nanofluid flow over a stretching cylinder with slip. *Alex. Eng. J.* **2017**, *56*, 671–677. [CrossRef]
39. Pandey, A.K.; Kumar, M. Natural convection and thermal radiation influence on nanofluid flow over a stretching cylinder in a porous medium with viscous dissipation. *Alex. Eng. J.* **2016**, *56*, 55–62. [CrossRef]
40. Sulochana, C.; Sandeep, N. Stagnation point flow and heat transfer behavior of Cu–water nanofluid towards horizontal and exponentially stretching/shrinking cylinders. *Appl. Nanosci.* **2016**, *6*, 451–459. [CrossRef]
41. Cao, Z.; Zhao, J.; Wang, Z.; Liu, F.; Zheng, L. MHD flow and heat transfer of fractional Maxwell viscoelastic nanofluid over a moving plate. *J. Mol. Fluids* **2016**, *222*, 1121–1127. [CrossRef]
42. Waini, I.; Ishak, A.; Pop, I. Nanofluid Flow on a Shrinking Cylinder with Al_2O_3 Nanoparticles. *Mathematics* **2021**, *9*, 14. [CrossRef]
43. Ho, C.J.; Liu, W.K.; Chang, Y.S.; Lin, C.C. Natural convection heat transfer of alumina-water nanofluid in vertical square enclosures: An experimental study. *Int. J. Therm. Sci.* **2010**, *49*, 1345–1353. [CrossRef]
44. Takabi, B.; Salehi, S. Augmentation of the heat transfer performance of a sinusoidal corrugated enclosure by employing hybrid nanofluid. *Adv. Mech. Eng.* **2014**, *6*, 147059. [CrossRef]
45. Subhani, M.; Nadeem, S. Numerical analysis of micropolar hybrid nanofluid. *Appl. Nanosci.* **2019**, *9*, 447–459. [CrossRef]
46. Khashi'ie, N.S.; Arifin, N.M.; Nazar, R.; Hafidzuddin, E.H.; Wahi, N.; Pop, I. Magnetohydrodynamics (MHD) axisymmetric flow and heat transfer of a hybrid nanofluid past a radially permeable stretching/shrinking sheet with Joule heating. *Chin. J. Phys.* **2020**, *64*, 251–263. [CrossRef]
47. Ghalambaz, M.; Rosca, N.C.; Rosca, A.V.; Pop, I. Mixed convection and stability analysis of stagnation-point boundary layer flow and heat transfer of hybrid nanofluids over a vertical plate. *Int. J. Numer. Methods Heat Fluid Flow* **2020**, *30*, 3737–3754. [CrossRef]
48. Mahanthesh, B.; Shehzad, S.A.; Ambreen, T.; Khan, S.U. Significance of Joule heating and viscous heating on heat transport of MoS2–Ag hybrid nanofluid past an isothermal wedge. *J. Therm. Anal. Calorim.* **2020**, *2*, 1221–1229. [CrossRef]
49. Mohammed, H.A.; Alawi Omer, A.; Wahid, M.A. Mixed convective nanofluid flow in a channel having backward-facing step with a baffle. *Powder Technol.* **2015**, *275*, 329–343. [CrossRef]
50. Nath, R.; Krishnan, M. Numerical study of double diffusive mixed convection in a backward facing step channel filled with Cu-water nanofluid. *Int. J. Mech. Sci.* **2019**, *153*, 48–63. [CrossRef]
51. Kherbeet, A.S.; Mohammed, H.A.; Ahmed, H.E.; Salman, B.H.; Alawi, O.A.; Safaei, M.R.; Khazaal, M.T. Mixed convection nanofluid flow over microscale forward-facing step—Effect of inclination and step heights. *Int. Commun. Heat Mass Transf.* **2016**, *78*, 145–154. [CrossRef]
52. Kherbeet, A.S.; Mohammed, H.A.; Salman, B.H.; Ahmed, H.E.; Alawi, O.A.; Rashidi, M.M. Experimental study of nanofluid flow and heat transfer over microscale backward- and forward-facing steps. *Exp. Therm. Fluid Sci.* **2015**, *65*, 13–21. [CrossRef]

53. Vijayalakshmi, A.; Srinivas, S.; Satyanarayana, B.; Reddy, S.A. Hydromagnetic pulsating flow of nanofluid between two parallel walls with porous medium. *Mater. Today Proc.* **2019**, *9*, 306–319. [CrossRef]
54. Zahmatkesh, I.; Torshizi, E. Scrutiny of Unsteady Flow and Heat Transfer in a Backward-Facing Step Under Pulsating Nanofluid Blowing Using the Eulerian-Eulerian Approach. *J. Mech.* **2019**, *35*, 93–105. [CrossRef]
55. Selimefendigil, F.; Öztop, H.F. MHD Pulsating forced convection of nanofluid over parallel plates with blocks in a channel. *Int. J. Mech. Sci.* **2019**, *157*, 726–740. [CrossRef]
56. Kumar, P.B.; Srinivas, S. Pulsating flow of a non-Newtonian nanofluid in a porous channel with magnetic field. *Mater. Today Proc.* **2019**, *2*, 320–332. [CrossRef]
57. Naphon, P.; Wiriyasart, S. Pulsating TiO2/water nanofluids flow and heat transfer in the spirally coiled tubes with different magnetic field directions. *Int. J. Heat Mass Transf.* **2017**, *115*, 537–543. [CrossRef]
58. Naphon, P.; Wiriyasart, S. Pulsating flow and magnetic field effects on the convective heat transfer of TiO2-water nanofluids in helically corrugated tube. *Int. J. Heat Mass Transf.* **2018**, *125*, 1054–1060. [CrossRef]
59. Selimefendigil, F.; Öztop, H.F. Forced convection and thermal predictions of pulsating nanofluid flow over a backward facing step with a corrugated bottom wall. *Int. J. Heat Mass Transf.* **2017**, *110*, 231–247. [CrossRef]
60. Chamkha, A.J.; Selimefendigil, F. Forced Convection of Pulsating Nanofluid Flow over a Backward Facing Step with Various Particle Shapes. *Energies* **2018**, *11*, 3068. [CrossRef]
61. Wang, F.-f.; Wu, S.-q.; Zhu, S.-l. Numerical simulation of flow separation over a backward-facing step with high Reynolds number. *Water Sci. Eng.* **2019**, *12*, 145–154. [CrossRef]
62. Xie, W.A.; Xi, G.N.; Zhong, M.B. Effect of the vortical structure on heat transfer in the transitional flow over a backward-facing step. *Int. J. Refrig.* **2017**, *74*, 465–474. [CrossRef]
63. Barkley, D.; Gabriela, M.; Gomes, M.; Henderson, R.D. Three-dimensional instability in flow over a backward-facing step. *J. Fluid Mech.* **2002**, *473*, 167–190. [CrossRef]
64. Rani, H.P.; Sheu, T.W.; Tsai, E.S. Eddy structures in a transitional backward-facing step flow. *J. Fluid Mech.* **2007**, *558*, 43–58. [CrossRef]
65. Alrashed, A.A.A.A.; Akbari, O.A.; Heydari, A.; Togharie, D.; Zarringhalam, M.; Shabani, G.A.S.; Seifi, A.R.; Goodarzi, M. The numerical modeling of water/FMWCNT nanofluid flow and heat transfer in a backward-facing contracting channel. *Phys. B Condens. Matter* **2018**, *537*, 176–183. [CrossRef]
66. Safaei, M.R.; Togun, H.; Vafai, K.; Kazi, S.N.; Badarudin, A. Investigation of Heat Transfer Enhancement in a Forward-Facing Contracting Channel Using FMWCNT Nanofluids. *Numer. Heat Transf. Part A Appl.* **2014**, *66*, 1321–1340. [CrossRef]
67. Brinkman, H.C. The Viscosity of Concentrated Suspensions and Solutions. *J. Chem. Phys.* **1952**, *20*, 571. [CrossRef]
68. Ho, C.J.; Chen, M.W.; Li, Z.W. Numerical simulation of natural convection of nanofluid in a square enclosure: Effects due to uncertainties of viscosity and thermal conductivity. *Int. J. Heat Mass Transf.* **2008**, *51*, 4506–4516. [CrossRef]
69. Yu, W.; Choi, S. The Role of Interfacial Layers in the Enhanced Thermal Conductivity of Nanofluids: A Renovated Maxwell Model. *J. Nanoparticle Res.* **2003**, *5*, 167–171. [CrossRef]
70. Ho, C.J.; Wei, L.C.; Li, Z.W. An experimental investigation of forced convective cooling performance of a microchannel heat sink with Al_22O3_3/water nanofluid. *Appl. Therm. Eng.* **2010**, *30*, 96–103. [CrossRef]
71. Klazly, M.M.; Bognar, G. CFD investigation of backward—Facing step nanofluid flow, MMCTSE 2020. *J. Phys. Conf. Ser.* **2020**, *1564*, 012010. [CrossRef]